# Physics & Diagnostics in Tokamaks Plasmas

# -

# Collective Scattering and Core Turbulence

**Cyrille Honoré** cyrille.honore@polytechnique.edu
Laboratoire de Physique des Plasmas
CNRS – SU – UPSaclay – ObsPM,
École Polytechnique – IP Paris
91128 Palaiseau cedex, France

# Turbulence and Confinement

The observed **energy confinement** in tokamak experiment is much worse than the expected confinement by the **neoclassical** model.

The experimental transport is evaluated from the plasma energy budget.

Typical **experimental** radial diffusion coefficient:

$$\chi_{\perp \exp} \sim 1\, m^2\, s^{-1}$$

Typical **neoclassical** radial diffusion coefficient:

$$\chi_{\perp NCi} \sim 5\ 10^{-2}\, m^2\, s^{-1}$$

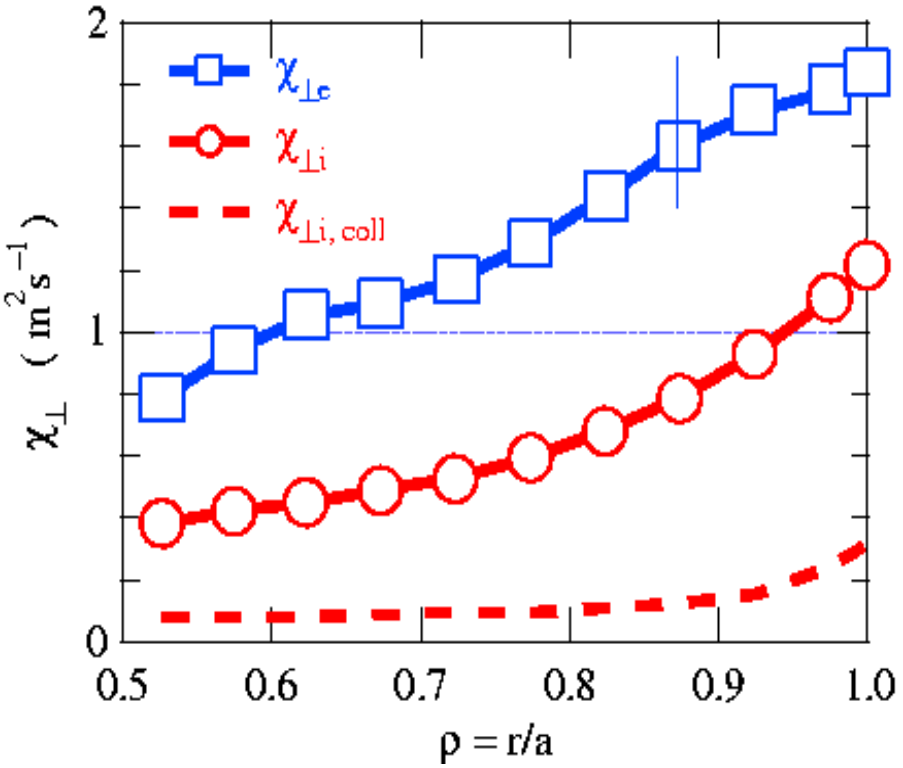

# Drift wave turbulence and transport

Plasma **small scale drift wave instabilities** are due to temperature and density gradients across the magnetic flux surfaces.
These instabilities induce plasma density and **potential peaks and sinks**.
The turbulent transport is generated partly by the **ExB drifts around these potential fluctuations**.
Plasma transport appears at the largest length scale of this drift wave turbulence.

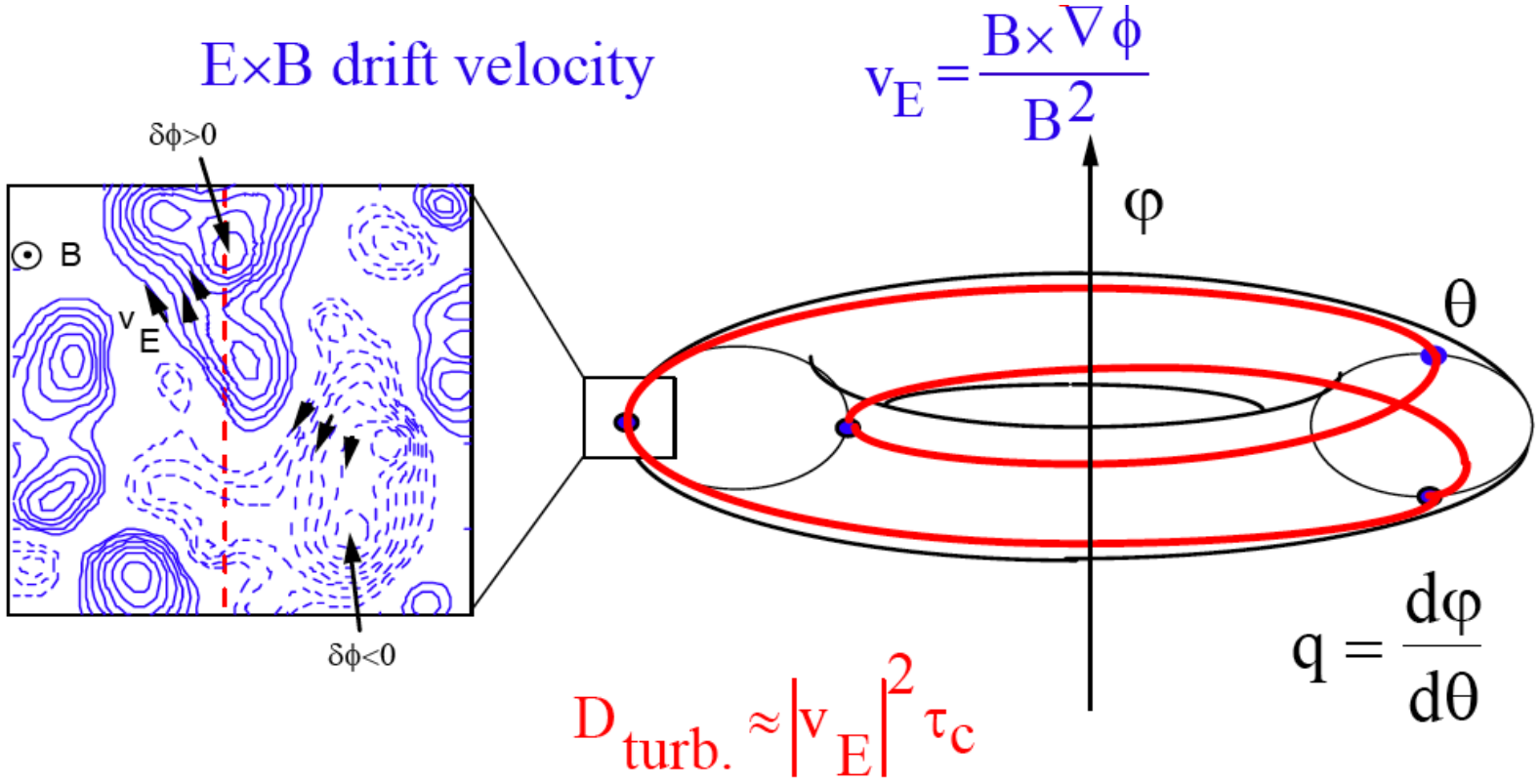

# Short scale fluctuations perpendicular to the magnetic field

Since charged particle are free to move along the magnetic field lines, **fluctuations have much longer parallel wavelength than perpendicular**.

$$k_{\parallel} \ll k_{\perp}$$

The **parallel component** of instabilities like drift waves nevertheless plays an important role for the drift stability through the parallel plasma collisionality

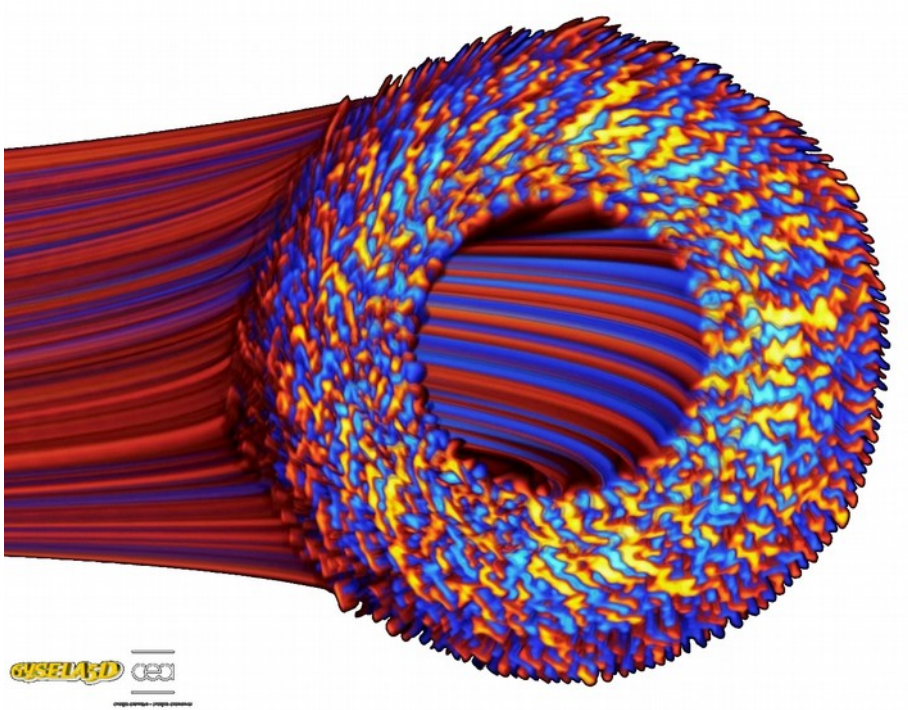

# Collective Scattering and Core Turbulence

- **Turbulence and confinement**
  - **Collective Thomson Scattering**
  - **Collective Scattering signal modulus and phase properties**
  - **Laser and Microwave Collective Scattering Instruments**
  - **Scattering Intensity and Turbulence wave number spectra**
  - **Scattering Doppler Frequency and Poloidal Velocity**
  - **H mode**
  - **Zonal flows and Geodesic Acoustic Modes**

# Collective Thomson Scattering

Scattering diagnostics are the main diagnostic to observe electrostatic instabilities in the plasma core.

# Thomson Diagnostics

Thomson scattering response depends on $k$ and $\omega$

$k\lambda_D > 1$ : Incoherent Thomson Scattering

The scattering signal spectrum reproduces electron velocity distribution

$$S_{\vec{k}}(\omega) = \frac{2\pi}{k} f_{e v_k}(-\omega/k)$$

$k\lambda_D < 1 \quad \omega_D \sim k v_{Ti}$ : Coherent (or collective) Thomson Scattering

The signal spectrum is an image of the ion velocity distribution

$$S_{\vec{k}}(\omega) = \frac{2\pi}{k}\left[\left|1 - \frac{\chi_e}{1+\chi_e+\chi_i}\right|^2 f_{v_k e}\left(\frac{-\omega}{k}\right) + \sum_i \left|\frac{-\chi_e}{1+\chi_e+\chi_i}\right|^2 Z_i^2 f_{v_k i}\left(\frac{-\omega}{k}\right)\right]$$

$k\lambda_D < 1 \quad \omega_D \sim k v_\varphi$ : Collective Thomson Scattering

the signal spectrum might correspond plasma instabilities with electron density fluctuations $(k, k v_\varphi)$

$$S_{\vec{k}}(\omega) = \frac{1}{T N_s}\left|n_{eT}(\vec{k}, \omega)\right|^2 \qquad n_{\vec{k}}(t) = \iiint_{V_s} n_e(\vec{r}, t)\, e^{-i\vec{k}.\vec{r}}\, d^3\vec{r}$$

# Thomson Scattering : scatterer sum

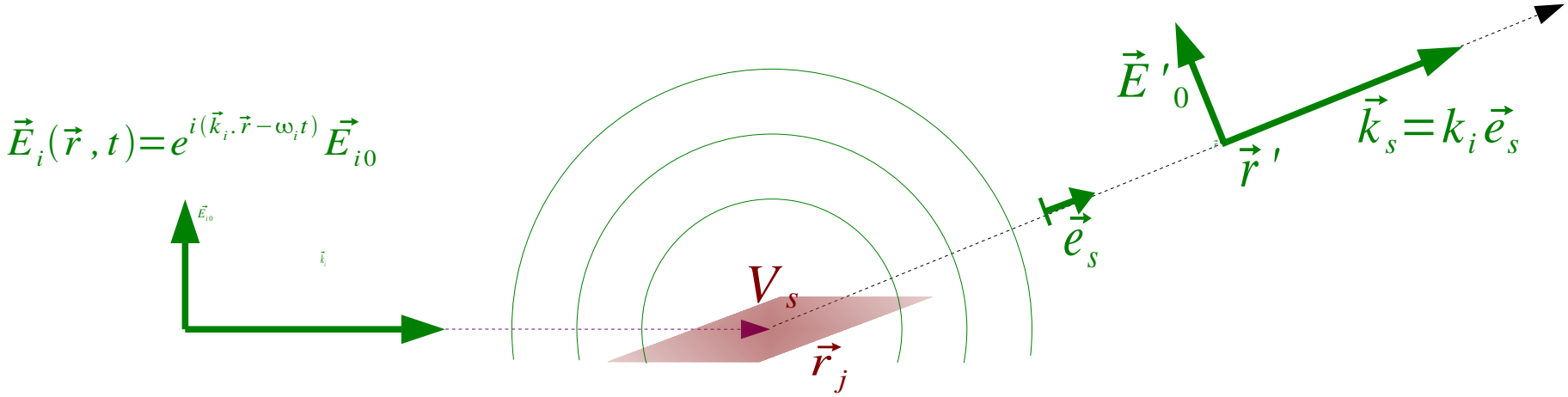


Scattered electric field sum upon $N_s = n_e V_s$ free electron scatterers:
(far field approximation)

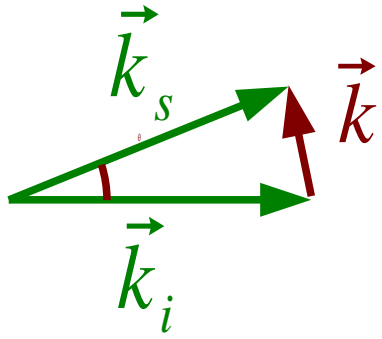


$$\vec{E}_s(\vec{r}',t)=\sum_{j=1}^{N_s}\vec{E}_{sj}(\vec{r}',t)$$

$$\vec{E}_s(\vec{r}',t)=r_0\frac{e^{i\vec{k}_s.\vec{r}'}}{r'}\vec{e}_s\wedge(\vec{e}_s\wedge\vec{E}_{i0})e^{-i\omega_i t}\sum_{j=1}^{N_s}e^{-i\vec{k}.\vec{r}_j(t)}$$

Each scatterer scattered electric field differs by **the scattering phase**.
The **scattering signal** will be defined by the sum of the scattering phases**:**

$$n_{\vec{k}}(t)=\sum_{j=1}^{N_s}e^{-i\vec{k}.\vec{r}_j(t)}$$

# Collective scattered field detection

Scattered field scatterer electron sum:

$$\vec{E}_s(\vec{r}\,',t)=r_0\frac{e^{i\vec{k}_s.\vec{r}\,'}}{r'}\vec{e}_s\wedge(\vec{e}_s\wedge\vec{E}_{i0})e^{-i\omega_i t}\sum_{j=1}^{N_s}e^{-i\vec{k}.\vec{r}_j(t)}$$

Expressed with fluid electron density ( $k\lambda_D<1$):

$$\vec{E}_s(\vec{r}\,',t)=r_0\frac{e^{i\vec{k}_s.\vec{r}\,'}}{r'}\vec{e}_s\wedge(\vec{e}_s\wedge\vec{E}_{i0})e^{-i\omega_i t}\iiint_{V_s}e^{-i\vec{k}.\vec{r}}n_e(\vec{r},t)d^3\vec{r}$$

**Doppler frequency** $\omega=k v_\varphi$ is **small** compared to incoherent Thomson $\omega=k v_{Te}$ and the **Scattering Signal time evolution** is important:
Spectrometers are not used to get Scattering Signal frequency properties.

Detector (**photodiode**) measures the electromagnetic power received on the detector surface $D$:

$$P_s(t)=\frac{N}{2\mu_0 C}\iint_D\left|\vec{E}_s(\vec{r}\,',t)\right|^2 d^2\vec{r}\,'\propto\langle E_{i0}{}^2\rangle\frac{r_0^2}{r'^2}\cos^2\theta_{pol}\left|n_{\vec{k}}(t)\right|^2$$

The **scattered power** is very weak.
Information on the **phase** of the Scattering Signal is lost : $n_{\vec{k}}(t)=\iiint_{V_s}n_e(\vec{r},t)e^{-i\vec{k}.\vec{r}}d^3\vec{r}$

# Heterodyne detection

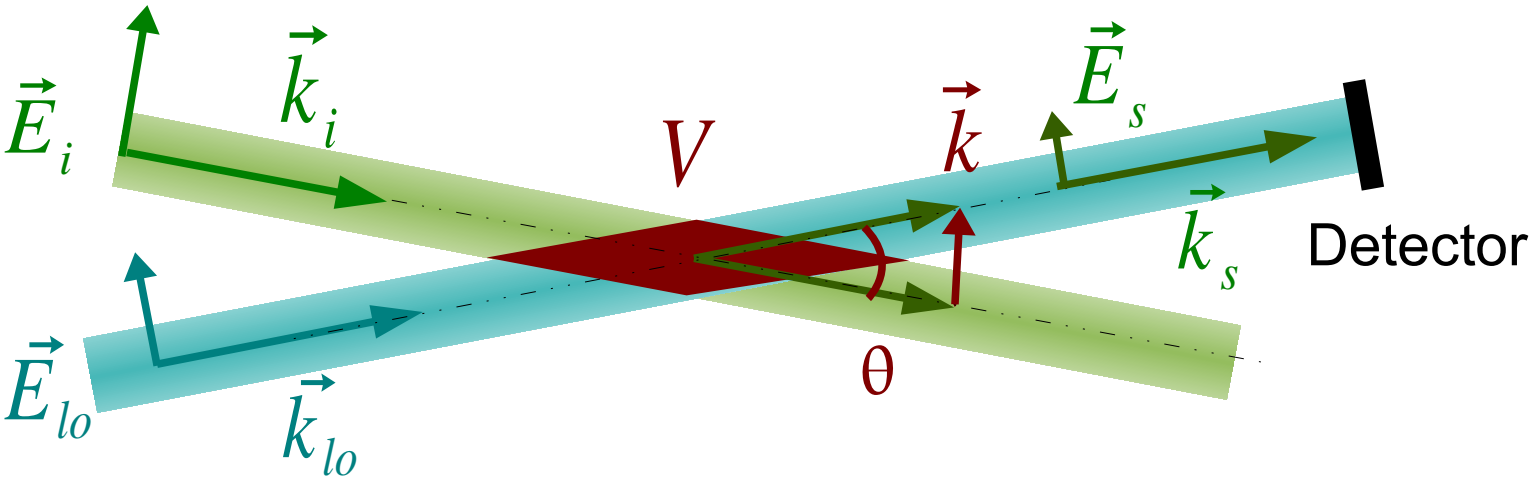


We use a **Local Oscillator** (**LO**) beam:

More intense than the scattered field:

$$\left|\vec{E}_{i0}\right| \gg \left|\vec{E}_{lo0}\right| \gg \left\langle \left|\vec{E}_s(\vec{r}\,',t)\right| \right\rangle$$

Same direction as the scattered field: $\vec{k}_{lo} \| \vec{k}_s$

**Same polarization** as the scattered field: $\vec{E}_{lo0} \| \vec{E'}_{i0} = \vec{e}_s \wedge (\vec{e}_s \wedge \vec{E}_{i0})$

**Coherent** with the incident field but with a **modulation frequency** shift:

$$\omega_i + \omega_m \qquad \omega_m \ll \omega_i \qquad k_{lo} \sim k_s = k_i$$

$$\vec{E}_{lo}(\vec{r}\,',t) = \mathrm{e}^{i[\vec{k}_{lo}.\vec{r}\,' - (\omega_i+\omega_m)t]} \vec{E}_{lo0}(r')$$

# Local Oscillator and Scattered electric field mixing

- The scattered and LO fields interfere on the detector:

$$\left|\vec{E}_s(\vec{r}\,',t)+\vec{E}_{lo}(\vec{r}\,',t)\right|^2=\left|\vec{E}_{lo}(\vec{r}\,',t)\right|^2+2\Re\left[\vec{E}^*_{lo}(\vec{r}\,',t).\vec{E}_s(\vec{r}\,',t)\right]+\left|\vec{E}_s(\vec{r}\,',t)\right|^2$$

- The electromagnetic power is a 3 term sum:

$$P_{tot}(t)=P_{lo}+P_b(t)+P_s(t)$$

  - the LO power (the largest but constant):

$$P_{lo}=\frac{N}{2\mu_0 C}\iint_D\left|\vec{E_{lo}}_0\right|^2 d^2\vec{r}\,'$$

  - the interference term (the largest fluctuating signal):

$$P_b(t)=\frac{N}{\mu_0 C}\iint_D\Re\left(\vec{E}^*_{lo}(\vec{r}\,',t).\vec{E}_s(\vec{r}\,',t)\right)d^2\vec{r}\,'$$

  - the scattered field power (negligible):

$$P_s(t)=\frac{N}{2\mu_0 C}\iint_D\left|\vec{E}_s(\vec{r}\,',t)\right|^2 d^2\vec{r}\,'$$

The interference term intensity: $\langle P_b(t)\rangle_t\le 2\sqrt{P_{lo}\langle P_s(t)\rangle_t}$

# Mixing term expression from scattering volume

**Scattered electric field** with incident field profile (reversing far field description):

$$\vec{E}_s(\vec{r}\,',t)=\iiint_{V_s} r_0 \frac{e^{ik_i|\vec{r}\,'-\vec{r}|}}{|\vec{r}\,'-\vec{r}|} e^{-i\omega_i t}\vec{E}\,'_{i0}(\vec{r})e^{i\vec{k}_i.\vec{r}}\,n_e(\vec{r},t)d^3\vec{r} \qquad \vec{E}\,'_{i0}(\vec{r})=\vec{e}_s\wedge(\vec{e}_s\wedge\vec{E}_{i0}(\vec{r}))$$

**LO electric field** backwards from the detector $\vec{E}_{lo}(\vec{r}\,')$ to the scattering volume $\vec{E}_{lo}(\vec{r})$, using Kirchhoff-Sommerfeld diffraction law:

$$\vec{E}_{lo}(\vec{r})=\frac{1}{i\lambda_i}\iint_D \frac{e^{ik_i|\vec{r}\,'-\vec{r}|}}{|\vec{r}\,'-\vec{r}|}\vec{E}_{lo}(\vec{r}\,')d^2\vec{r}\,' \qquad \vec{E}_{lo}(\vec{r}\,',t)=e^{i[\vec{k}_{lo}.\vec{r}\,'-(\omega_i+\omega_m)t]}\vec{E}_{lo0}(\vec{r}\,')$$

**Mixing term** (using both expressions):

$$P_b(t)=\frac{N}{\mu_0 C}\iint_D \Re\left(\vec{E}^*_{lo}(\vec{r}\,',t).\vec{E}_s(\vec{r}\,',t)\right)d^2\vec{r}\,'$$

$$P_b(t)=\frac{N}{\mu_0 C}\iint_D \Re\left(\vec{E}^*_{lo}(\vec{r}\,',t).\iiint_{V_s} r_0\frac{e^{ik_i|\vec{r}\,'-\vec{r}|}}{|\vec{r}\,'-\vec{r}|}e^{-i\omega_i t}\vec{E}\,'_{i0}(\vec{r})e^{i\vec{k}_i.\vec{r}}\,n_e(\vec{r},t)d^3\vec{r}\right)d^2\vec{r}\,'$$

$$P_b(t)=\Re\left\{i\frac{r_0\lambda_i}{\mu_0 C}e^{i\omega_m t}\iiint_{V_s}\vec{E}_{lo0}(\vec{r})e^{-i\vec{k}_s.\vec{r}}.\vec{E}\,'_{i0}(\vec{r})e^{i\vec{k}_i.\vec{r}}\,n_e(\vec{r},t)d^3\vec{r}\right\}$$

# Beam profile

$$P_b(t)=\Re\{i\frac{r_0\lambda_i}{\mu_0 C}e^{i\omega_m t}\iiint_{V_s}\vec{E}_{lo0}(\vec{r})e^{-i\vec{k}_s.\vec{r}}.\vec{E}'_{i0}(\vec{r})e^{i\vec{k}_i.\vec{r}}n_e(\vec{r},t)d^3\vec{r}\}$$

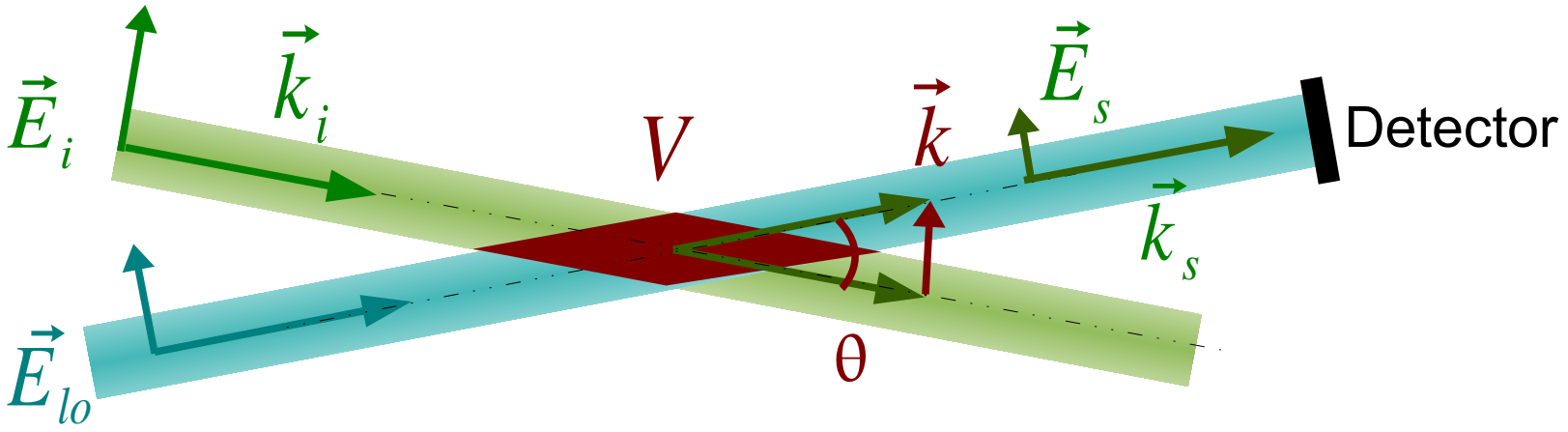


Volume integration is weighted by the crossing of both incident and LO beams

The beams are described by their profiles:

$$u_i(\vec{r})=\frac{1}{E_{iM}}E_{i0}(\vec{r})=\frac{1}{E'_{iM}}E'_{i0}(\vec{r}) \qquad E'_{i0}(\vec{r})=u_i(\vec{r})E'_{iM} \qquad E'_{iM}=max(E'_{i0}(\vec{r})) \qquad 0\le u_i(\vec{r})\le 1$$

$$u_{lo}(\vec{r})=\frac{1}{E_{olM}}E_{lo0}(\vec{r}) \qquad E_{lo0}(\vec{r})=u_{lo}(\vec{r})E_{olM} \qquad E'_{loM}=max(E'_{lo0}(\vec{r}))$$

Scattering volume profile is described by the product of both profiles:

$$u(\vec{r})=u_{lo}(\vec{r})u_i(\vec{r}) \qquad V_s=\iiint u(\vec{r})^2 d^3\vec{r}$$

Wave mixing term includes the Fourier transform of the electron density weighted by the Scattering volume profile:

$$P_b(t)=\Re\{i\frac{r_0\lambda_i}{\mu_0 C}e^{i\omega_m t}\vec{E}_{loM}.\vec{E}'_{iM}\iiint u(\vec{r})n_e(\vec{r},t)e^{-i\vec{k}.\vec{r}}d^3\vec{r}\}$$

# Detector current

The detector is a photovoltaic diode : an electron is sent for each received photon :

$$i(t)=\frac{\eta q_e}{\hbar \omega_i} P(t)$$

Detector quantum efficiency: $\eta$

The received electromagnetic power:

$$P_{tot}(t)=P_{lo}+P_b(t)+P_s(t)$$

The LO current is proportional to the LO constant power:

$$i_{lo}=\frac{\eta q_e}{\hbar \omega_i} P_{lo}$$

The mixing term signal is a fluctuating signal modulated at $\omega_m$ :

$$i_b(t)=\Re\left\{ i \frac{\varepsilon_0 r_0 \lambda_i^2 \eta q_e}{h} \vec{E}_{loM} . \vec{E}'_{iM} e^{i\omega_m t} \iiint u(\vec{r}) n_e(\vec{r},t) e^{-i\vec{k}.\vec{r}} d^3\vec{r} \right\}$$

The scattered electric power is negligible: $i_{tot}(t)=i_{lo}+i_b(t)$

Scattering signal: $n_{\vec{k}}(t)=\iiint u(\vec{r}) n_e(\vec{r},t) e^{-i\vec{k}.\vec{r}} d^3\vec{r}$ $\qquad n_{\vec{k}}(t)=\iiint_{V_s} n_e(\vec{r},t) e^{-i\vec{k}.\vec{r}} d^3\vec{r}$

# Finite volume and scattering wave number resolution

The Scattering signal depends on the Scattering volume profile $u(\vec{r}) = u_{lo}(\vec{r})\, u_i(\vec{r})$

$$i_b(t) = \Re\left\{ i \frac{\varepsilon_0 r_0 \lambda_i^2 \eta q_e}{h} \vec{E}_{loM} . \vec{E}'_{iM} e^{i\omega_m t} \iiint u(\vec{r}) n_e(\vec{r}, t) e^{-i\vec{k}.\vec{r}} d^3\vec{r} \right\}$$

Both beams have a Gaussian profile:

$$u_x(x, y, z) = e^{-(y^2+z^2)/w^2}$$

$w$ : Gaussian beam waist

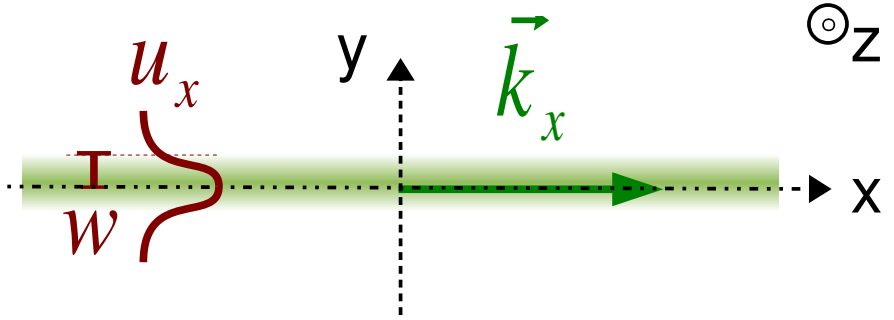


Each beam electric field:

$$\vec{E}_x(\vec{r}', t) = e^{i(k_x x - \omega_x t)} \vec{E}_{x0}(\vec{r}) = e^{i(k_x x - \omega_x t)} e^{-(y^2+z^2)/w^2} \vec{E}_{xM}$$

Each beam electromagnetic power:

$$P_x = \frac{\pi w^2 N}{4\mu_0 C} E_{xM}^2$$

# Scattering volume profile

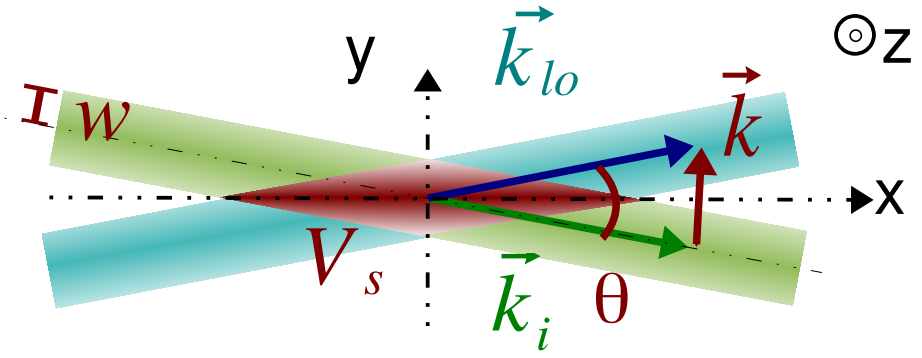


The incident and LO beam crossing volume:

$$u_i(x,y,z)=\mathrm{e}^{-[(y\cos\theta/2-x\sin\theta/2)^2+z^2]/w^2}$$

$$u_{lo}(x,y,z)=\mathrm{e}^{-[(y\cos\theta/2+x\sin\theta/2)^2+z^2]/w^2}$$

Assuming $\theta \ll 1$, the scattering volume profile:

$$u(x,y,z)=u_i(x,y,z)u_{lo}(x,y,z)=\mathrm{e}^{-x^2\theta^2/2w^2-2y^2/w^2-2z^2/w^2}$$

The volume size for each direction is evaluated using integrated length:

$$l=\frac{1}{max(u^2)}\int_{-\infty}^{+\infty}u(\zeta)^2\,d\zeta$$

For both transverse directions:

$$L_{trans}=\frac{\sqrt{\pi}\,w}{2}$$

For longitudinal direction, volume length depends on $\theta$:

$$L_{long}=\frac{\sqrt{\pi}\,w}{\theta}$$

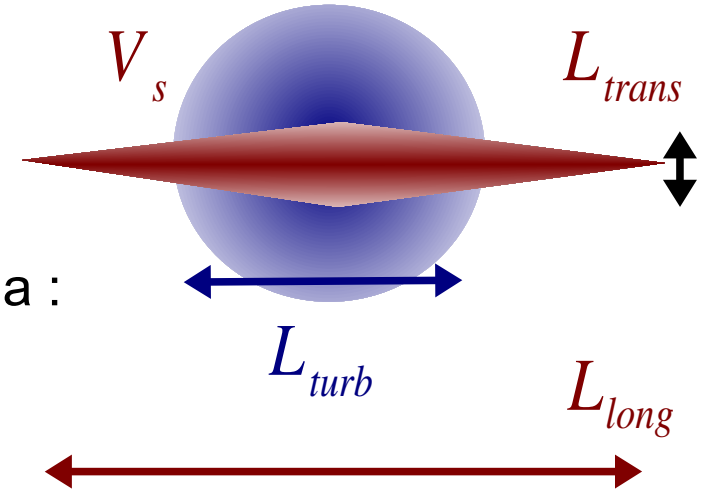


This scattering volume length might be longer than the plasma : the scattering volume length is replaced with the intercepted plasma length $L_{turb}$

$$V_{turb}=\frac{\pi w^2}{4}L_{turb}$$

# Finite Volume and finite wave number resolution

Scattering signal definition using Scattering volume profile:

$$n_{\vec{k}}(t)=\iiint u(\vec{r})\,\mathrm{e}^{-i\vec{k}.\vec{r}}\,n_e(\vec{r},t)\,d^3\vec{r}$$

Fourier transform of a product is the convolution of Fourier transforms:

$$n_{\vec{k}}(t)=\frac{1}{(2\pi)^3}\iiint u(\vec{k}-\vec{k}')\,n_e(\vec{k}',t)\,d^3\vec{k}'$$

$n_e(\vec{k},t)$ is the whole space electron density Fourier Transform:

$$n_e(\vec{k},t)=\iiint \mathrm{e}^{-i\vec{k}.\vec{r}}\,n_e(\vec{r},t)\,d^3\vec{r}$$

$u(\vec{k})$ is the Fourier transform of the profile:

$$u(\vec{k})=\iiint u(\vec{r})\,\mathrm{e}^{-i\vec{k}.\vec{r}}\,d^3\vec{r}$$

It has a Gaussian shape:

$$u(k_x,k_y,k_z)=\frac{(2\pi)^{3/2}w^3}{4\theta}\,\mathrm{e}^{-k_x^2w^2/2\theta^2-k_y^2w^2/8-k_z^2w^2/8}$$

The finite scattering volume induces a finite resolution.

# Typical wave number resolution

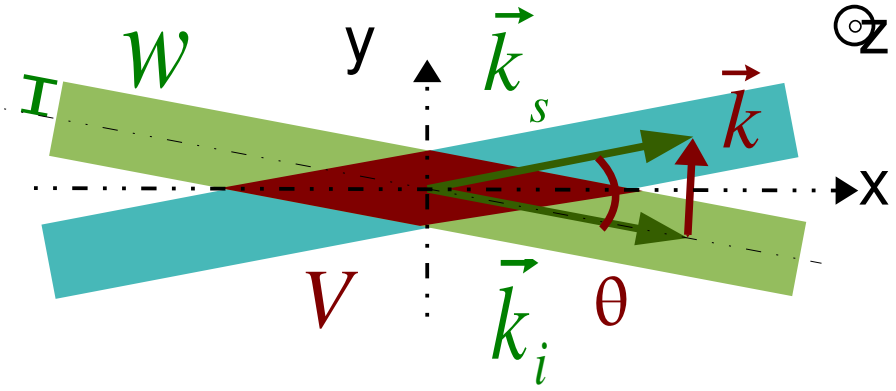


$$u(k_x,k_y,k_z)=\frac{(2\pi)^{3/2}w^3}{4\theta}e^{-k_x^2w^2/2\theta^2-k_y^2w^2/8-k_z^2w^2/8}$$

$$u(x,y,z)=e^{-x^2\theta^2/2w^2-2y^2/w^2-2z^2/w^2}$$

Absolute wave number resolution

transverse resolution: $dk_t=\frac{\sqrt{2}}{w}$

longitudinal resolution: $dk_l=\frac{\sqrt{\pi}}{L_{turb}\sqrt{2}}$

Wave number relative resolution (better for larger wave number)

transverse resolution: $\frac{dk_t}{k}=\frac{\sqrt{2}}{kw}=\frac{\lambda}{\sqrt{2}\pi w}$

For $\lambda/w=0.5$ : $dk_t/k\sim 0.11$

The finite k resolution has a widening effect:

$$n_{\vec{k}}(t)=\frac{1}{(2\pi)^3}\iiint u(\vec{k}-\vec{k}')n_e(\vec{k}',t)d^3\vec{k}'$$

# Collective Thomson Scattering Modulus and Phase

# Scattering signal intensity

$$n_{\vec{k}}(t)=\sum_{j=1}^{N_s} e^{-i\vec{k}.\vec{r}_j(t)}$$

**Lower limit: the incoherent** Thomson scattering :

$$\left\langle \left| n_{\vec{k}}(t) \right|^2 \right\rangle_t = \left\langle \sum_j \sum_l e^{-i\vec{k}.[\vec{r}_j(t)-\vec{r}_l(t)]} \right\rangle_t = \left\langle \sum_j e^{-i\vec{k}.\vec{0}} \right\rangle_t = N_s \qquad \left\langle \sum_j \sum_{l\neq j} e^{-i\vec{k}.[\vec{r}_j(t)-\vec{r}_l(t)]} \right\rangle_t \sim 0$$

Static Form Factor : $S_{\vec{k}}=\dfrac{\left\langle \left| n_{\vec{k}}(t) \right|^2 \right\rangle_t}{N_s}=1$

**Upper limit: the completely coherent case.**

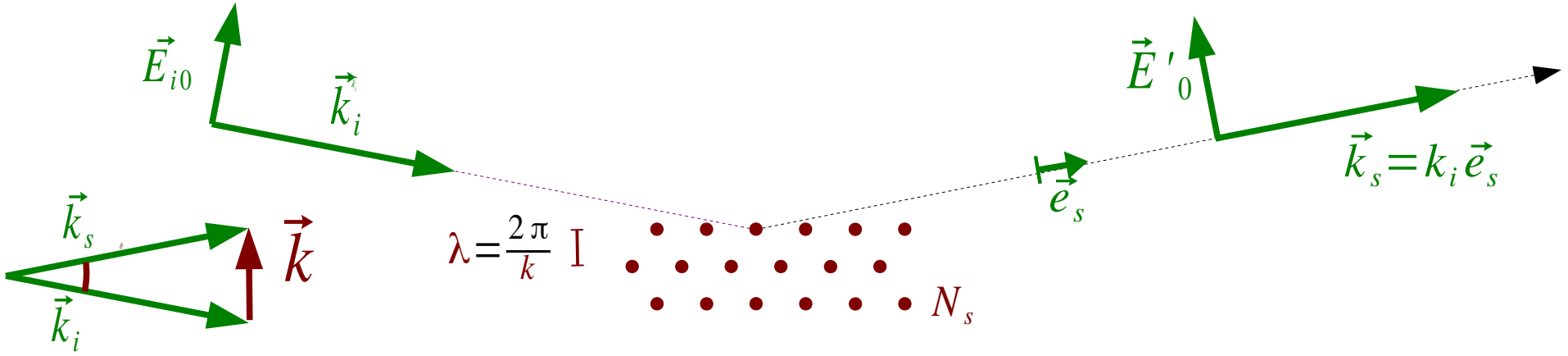


All scatterers produces the same phase (for a crystal) $\quad n_{\vec{k}}(t)=N_s e^{-i\varphi(t)}$

$$\left\langle \left| n_{\vec{k}}(t) \right|^2 \right\rangle_t = N_s^2 \qquad S_{\vec{k}}=\frac{\left\langle \left| n_{\vec{k}}(t) \right|^2 \right\rangle_t}{N_s}=N_s$$

The Static form factor is the number
of scatterers inside the coherent structure.
The coherent structure have a large enhancing effect on scattering.

# Scattering signal intensity

**Reality: the scattering signal is the sum of uncorrelated coherent structures**

$n_s$ structures, each with $N_s/n_s$ scatterers.

$$n_{\vec{k}}(t)=\sum_{l=1}^{n_s} n_{\vec{k}\,l}(t) \qquad n_{\vec{k}\,1}(t)=\sum_{j=1}^{N_s/n_s} e^{-i\vec{k}.\vec{r}_j(t)} \qquad n_{\vec{k}\,l}(t)=\sum_{j=1+(l-1)N_s/n_s}^{lN_s/n_s} e^{-i\vec{k}.\vec{r}_j(t)}$$

$$j\neq l \qquad \langle n_{\vec{k}\,j}(t)\,n^{*}_{\vec{k}\,l}(t+\tau)\rangle_t \ll \langle |n_{\vec{k}\,j}(t)|\,|n_{\vec{k}\,l}(t+\tau)|\rangle_t \qquad \langle |n_{\vec{k}\,l}(t)|^2\rangle_T \ll \frac{N_s^2}{n_s^2}$$

The **static form factor** is of the **average scatterer number** that form a coherent structure $l$:

$$S_{\vec{k}}=\frac{\langle |n_{\vec{k}}(t)|^2\rangle_t}{N_s}=\frac{1}{N_s}\sum_{l=1}^{n_s}\langle |n_{\vec{k}\,l}(t)|^2\rangle_t \qquad \sum_{l=1}^{n_s}\langle |n_{\vec{k}\,l}(t)|^2\rangle_t \ll n_s\frac{N_s^2}{n_s^2}$$

Because of this **collective effect**, Scattering signal is much more easier to detect than incoherent or coherent scattering signal.

$$1<S_{\vec{k}}\ll\frac{N_s}{n_s}$$

Analogy with poly-crystals:
The static form factor is the average number of scatterers inside each crystal coherent structure.
The scattering signal $n_{\vec{k}\,l}(t)$ from distinct crystals are not correlated.

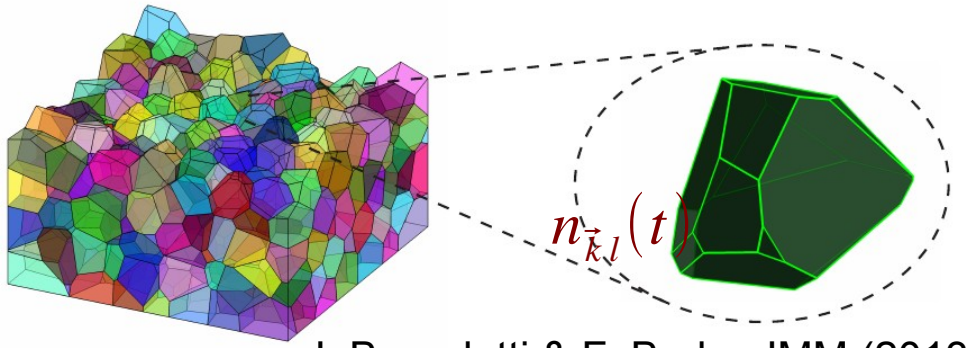


I. Benedetti & F. Barbe JMM (2013)

# Scattering signal correlation and structure displacement

The scattering signal is the sum of signals from different coherent structures:

$$n_{\vec{k}}(t)=\sum_l n_{\vec{k}l}(t)$$

The coherent structures are uncorrelated from each other:

$$j\neq l \qquad \langle n_{\vec{k}j}(t)\,n^*_{\vec{k}l}(t+\tau)\rangle_t \ll \langle |n_{\vec{k}j}(t)|\,|n_{\vec{k}l}(t+\tau)|\rangle_t$$

Each structure is **convected** by the large scales of the flow

$\vec{\Delta}_l(t,\tau)$ is the large scale displacement between time $t$ and $t+\tau$

$$n_{\vec{k}l}(t+\tau)=\iiint_{V_s} e^{-i\vec{k}.\vec{r}}\, n_{\vec{k}l}(\vec{r},t+\tau)\,d^3\vec{r}$$

We assume each structure is frozen between $t$ and $t+\tau$

$$n_{\vec{k}l}(t+\tau)=\iiint_{V_s} e^{-i\vec{k}.\vec{r}}\, n_l(\vec{r}-\vec{\Delta}_l(t,\tau),t)\,d^3\vec{r}$$

Substitution : $\vec{r}=\vec{r}\,'+\vec{\Delta}_l(t,\tau)$

$$n_{\vec{k}l}(t+\tau)=\iiint_{V_s} e^{-i\vec{k}.[\vec{r}\,'+\vec{\Delta}_l(t,\tau)]}\, n_l(\vec{r}\,',t)\,d^3\vec{r}\,'$$

$$n_{\vec{k}l}(t+\tau)=n_{\vec{k}l}(t)\,e^{-i\vec{k}.\vec{\Delta}_l(t,\tau)}$$

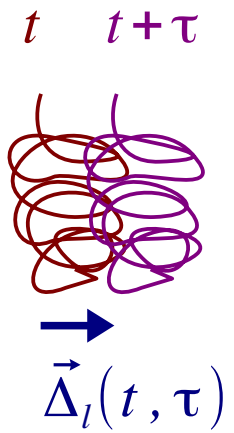

# Signal correlation and coherent structure displacement

Scattering signal time correlation

$$C(\vec{k},\tau)=\frac{1}{N_s}\langle n_{\vec{k}}(t)\,n^{*}_{\vec{k}}(t+\tau)\rangle_T$$

$$C(\vec{k},\tau)=\frac{1}{N_s}\langle \sum_j n_{\vec{k}\,j}(t)\sum_l n^{*}_{\vec{k}\,l}(t+\tau)\rangle_t$$

there is no correlation between structures: $j\neq l$ $\quad \langle n_{\vec{k}\,j}(t)\,n^{*}_{\vec{k}\,l}(t+\tau)\rangle_t \ll \langle |n_{\vec{k}\,j}(t)|\,|n_{\vec{k}\,l}(t+\tau)|\rangle_t$

$$C(\vec{k},\tau)=\frac{1}{N_s}\sum_l \langle n_{\vec{k}\,l}(t)\,n^{*}_{\vec{k}\,l}(t+\tau)\rangle_t$$

$$C(\vec{k},\tau)=\frac{1}{N_s}\sum_l \langle |n_{\vec{k}\,l}(t)|^2\, e^{i\vec{k}.\vec{\Delta}_l(t,\tau)}\rangle_t$$

$$n_{\vec{k}\,l}(t+\tau)=n_{\vec{k}\,l}(t)\,e^{-i\vec{k}.\vec{\Delta}_l(t,\tau)}$$

**We assume displacement is independent from the structure static form factor.**

All coherent structures follow the same displacement probability distribution.

$$C(\vec{k},\tau)=\frac{1}{N_s}\langle e^{i\vec{k}.\vec{\Delta}(\tau)}\rangle\sum_l \langle |n_{\vec{k}\,l}(t)|^2\rangle$$

The time correlation is the product of 2 effects:

$$C(\vec{k},\tau)=S(\vec{k})\,\langle e^{i\vec{k}.\vec{\Delta}(t,\tau)}\rangle_t$$

- $S(\vec{k})$ : **static form factor** (constant)
- $\langle e^{i\vec{k}.\vec{\Delta}(t,\tau)}\rangle_t$ : **structure displacement characteristic function** $\vec{\Delta}(t,\tau)$

# Coherent structures uniform movement

For delays shorter than the correlation time, we assume the **Taylor hypothesis** applied on each coherent structure:

$\vec{U}(t)$ : structure large scale common velocity (varies for long times)

Uniform short time displacement: $\vec{\Delta}(\vec{r},t,\tau)=\vec{U}(t)\tau$

Velocity component along: $\vec{k}$ $\quad U_{\vec{k}}(t)=\vec{U}(t).\vec{e}_k \quad \vec{e}_k=\frac{1}{k}\vec{k}$

Scattering signal time correlation

$$C(\vec{k},\tau)=S(\vec{k})\left\langle e^{ikU_{\vec{k}}(t)\tau}\right\rangle_t$$

$P_{U\vec{k}}$ : probability distribution of coherent structure velocity component along $\vec{k}$

Ergodic hypothesis: $\left\langle F[x(t)]\right\rangle_T=\int dx' P_x(x')F(x')$

$$C(\vec{k},\tau)=S(\vec{k})\int du\, P_{U\vec{k}}(u)e^{iku\tau}$$

$$S(\vec{k},\omega)=\frac{2\pi}{k}S(\vec{k})P_{U_{\vec{k}}}\left(\frac{-\omega}{k}\right)$$

Frequency spectra are similar to the incoherent case, but apply to large scale structures.

# Uniform motion and diffusion

Scattering signal time correlation as characteristic function of the coherent structure displacement:

$$C_{\vec{k}}(\tau) \propto \langle e^{i\vec{k}.\vec{\Delta}(\vec{r},t,\tau)} \rangle_t = \int d^3\vec{\Delta}\, P(\vec{\Delta})\, e^{i\vec{k}.\vec{\Delta}}$$

displacement Gaussian distribution: $P(\vec{\Delta}) = \frac{1}{\sqrt{(2\pi)^3 \langle \tilde{\vec{\Delta}}^2 \rangle}} e^{-(\vec{\Delta}-\langle\vec{\Delta}\rangle)^2/2\langle\tilde{\vec{\Delta}}^2\rangle}$ $\qquad \vec{\Delta} = \langle\vec{\Delta}\rangle + \tilde{\vec{\Delta}}$

Displacement is the velocity time integration: $\vec{\Delta} = \int_t^{t+\tau} \vec{U}\, dt$

Mean displacement: $\langle\vec{\Delta}\rangle = \langle\vec{U}\rangle \tau$

Fluctuation part: $\tilde{\vec{\Delta}} = \int_t^{t+\tau} dt\, \tilde{\vec{U}}(t)$ $\qquad \vec{U} = \langle\vec{U}\rangle + \tilde{\vec{U}}$

$$\langle\tilde{\vec{\Delta}}^2\rangle = \langle \int_t^{t+\tau} dt_1 \int_t^{t+\tau} dt_2\, \tilde{\vec{U}}(t_1)\tilde{\vec{U}}(t_2)\rangle = 2\int_0^{\tau} (\tau-\tau')\langle\tilde{\vec{U}}(t)\tilde{\vec{U}}(t+\tau')\rangle_t d\tau' \qquad t_2 = t_1 + \tau'$$

The velocity time correlation decrease exponentially on time $\tau_L$:

$$\langle\tilde{\vec{U}}(t)\tilde{\vec{U}}(t+\tau)\rangle_t = \langle\tilde{\vec{U}}^2\rangle e^{-\tau/\tau_L}$$

Displacement variance:

$$\langle\tilde{\vec{\Delta}}^2\rangle = 2\langle\tilde{\vec{U}}^2\rangle \tau_L^2 \left(\frac{\tau}{\tau_L} + e^{-\tau/\tau_L} - 1\right)$$

# Uniform motion and diffusion

Displacement correlation $\langle \widetilde{\vec{\Delta}^2} \rangle = 2 \langle \widetilde{\vec{U}^2} \rangle \tau_L^2 \left( \frac{\tau}{\tau_L} + e^{-\tau/\tau_L} - 1 \right)$ $\qquad \langle \vec{\Delta} \rangle = \langle \vec{U} \rangle \tau$

$\tau \ll \tau_L \Rightarrow \langle \widetilde{\vec{\Delta}^2} \rangle = \langle \widetilde{\vec{U}^2} \rangle \tau^2$ Uniform displacement

$\tau \gg \tau_L \Rightarrow \langle \widetilde{\vec{\Delta}^2} \rangle = 2 \langle \widetilde{\vec{U}^2} \rangle \tau_L \tau$ Diffusive displacement $D = \langle \widetilde{\vec{U}^2} \rangle \tau_L$

Coherent structure displacement characteristic function:

$$\left\langle e^{i\vec{k}.\vec{\Delta}(\vec{r},t,\tau)} \right\rangle_t = e^{i\vec{k}.\langle\vec{\Delta}\rangle - \frac{1}{2}k^2 \langle \widetilde{\vec{\Delta}^2} \rangle}$$

$$P(\vec{\Delta}) = \frac{1}{\sqrt{(2\pi)^3 \langle \widetilde{\vec{\Delta}^2} \rangle}} e^{-(\vec{\Delta} - \langle\vec{\Delta}\rangle)^2 / 2 \langle \widetilde{\vec{\Delta}^2} \rangle}$$

Scattering Signal time correlation has a **Taylor function** expression :

$$C_{\vec{k}}(\tau) = S(\vec{k}) \left\langle e^{i\vec{k}.\vec{\Delta}(\vec{r},t,\tau)} \right\rangle_t = S(\vec{k}) e^{i\vec{k}.\langle\vec{U}\rangle\tau} e^{-k^2 \langle \widetilde{\vec{U}^2} \rangle \tau_L^2 \left( \frac{\tau}{\tau_L} + e^{-\tau/\tau_L} - 1 \right)}$$

Scattering signal frequency spectrum : $S_{\vec{k}}(\omega) = \int d\tau \, C_{\vec{k}}(\tau) e^{i\omega\tau}$

- no algebraic expression for the general case,
- Gaussian shape for the uniform displacement limit $\tau_{C_{\vec{k}}} \ll \tau_L$
- Lorentzian shape for the diffusive displacement limit $\tau_{C_{\vec{k}}} \gg \tau_L$

The scattering signal frequency may not reproduce the structure velocity distribution

# Collective Thomson Scattering time signal

## Typical collective Scattering time signals

Real and imaginary parts, and modulus

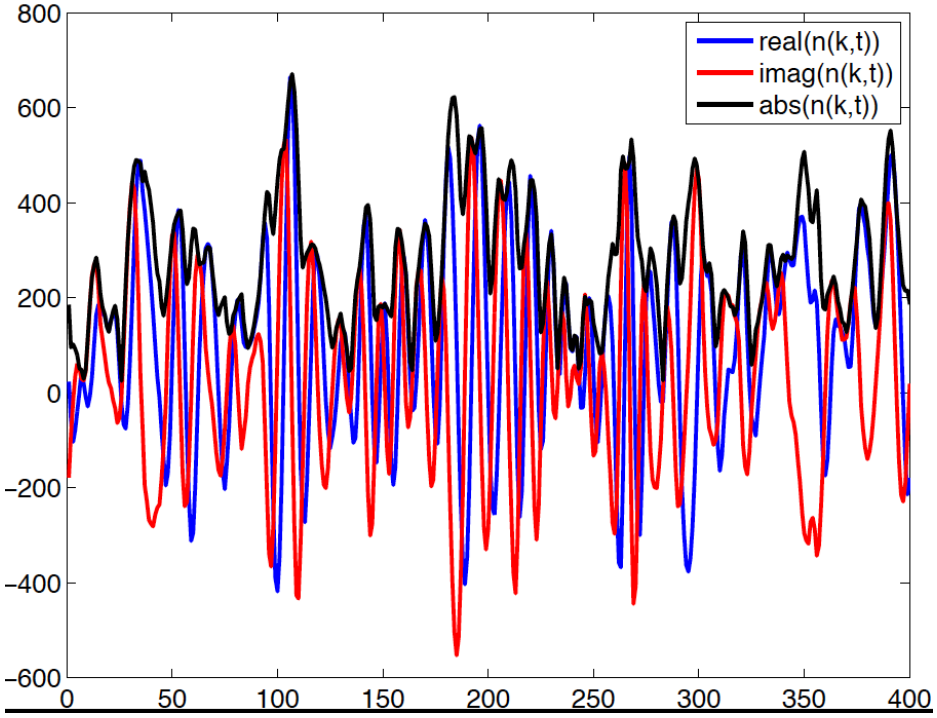


Complex plane

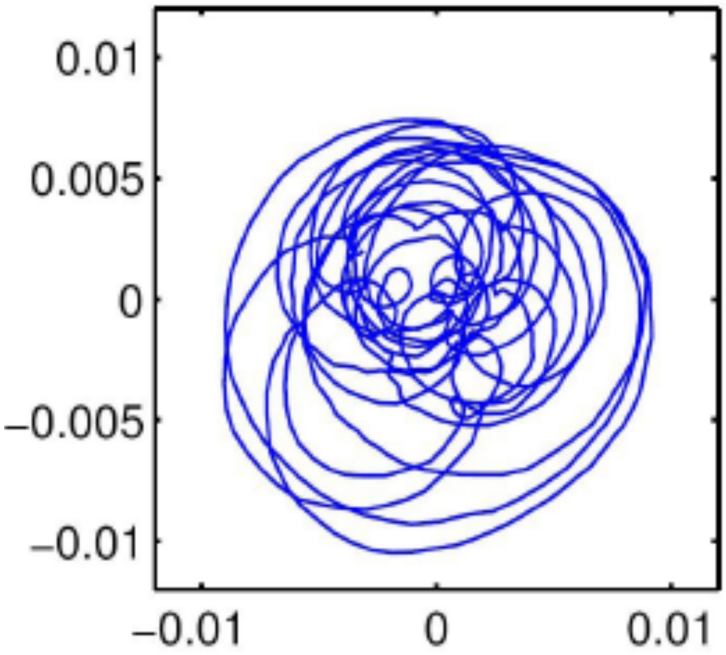


**Modulus time variation** are linked to the coherent structure **life time** or **flight time** across the scattering volume.

**Phase rotation** are linked to the coherent structure **displacement** across the scattering volume.

$$n_{\vec{k}\,l}(t+\tau) \sim n_{\vec{k}\,l}(t)\, \mathrm{e}^{-i\vec{k}.\vec{\Delta}_l(t,\tau)}$$

# Collective Thomson Scattering Instruments

# Laser Collective Thomson Forward Scattering : Tore Supra

ALTAIR :

CW CO2 laser : $\lambda_i = 10{,}6\ \mu m$ $10\ W$

$\omega_i \gg \omega_p$ $\omega_i \gg \omega_{ce}$

Forward Scattering

$0.45 \leq \theta \leq 4.5\ mrad$ $1° \sim 17.45\ mrad$

Wavelength range :

$0.2 \leq \lambda \leq 2\ cm$

Beams are crossing the Tokamak

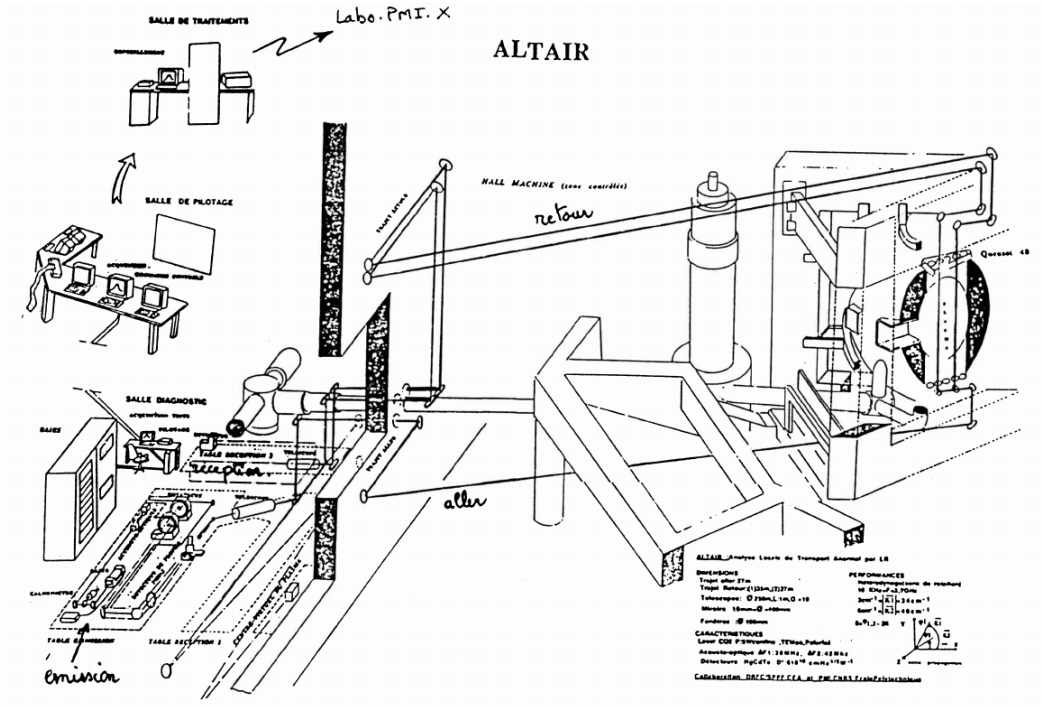


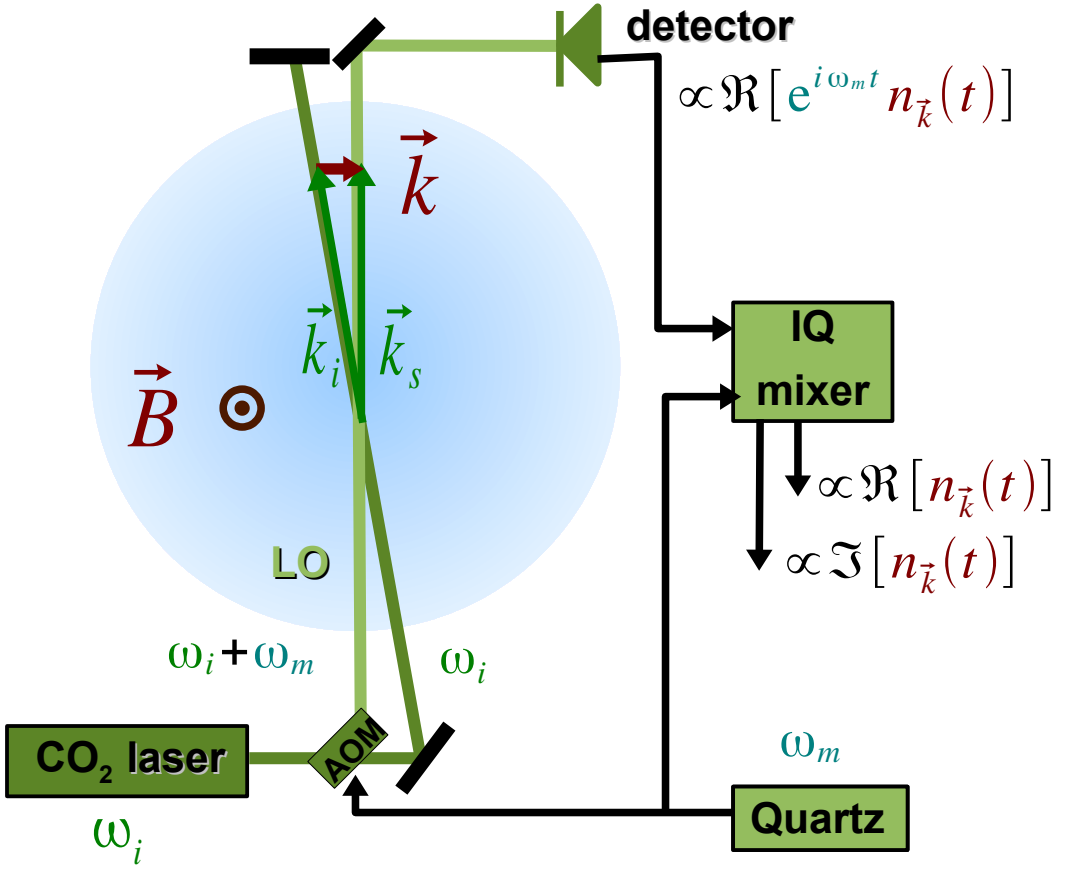


Truc et al.,Rev. of Scientific Instruments, **63(7)**, p 3716 (1992)

# Laser Collective Thomson Forward Scattering

The Scattering angle is very small:
the Scattering volume $V_s$ crosses the whole plasma.

The condition $\vec{k} \perp \vec{B}$ allows to reduce the effective volume.

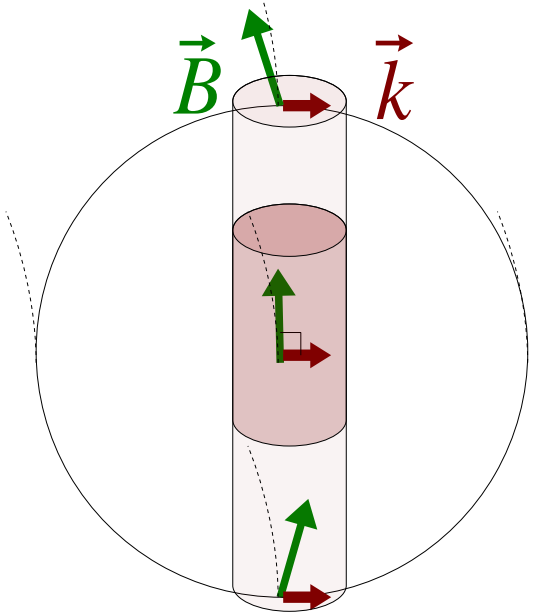


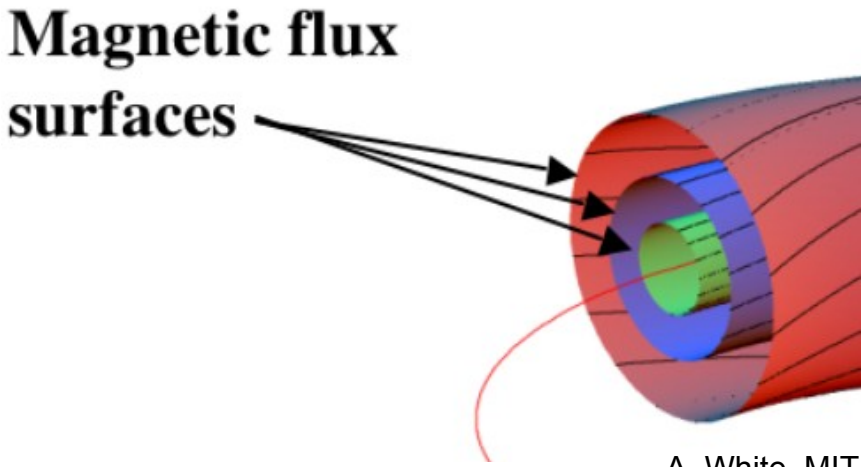


A. White, MIT

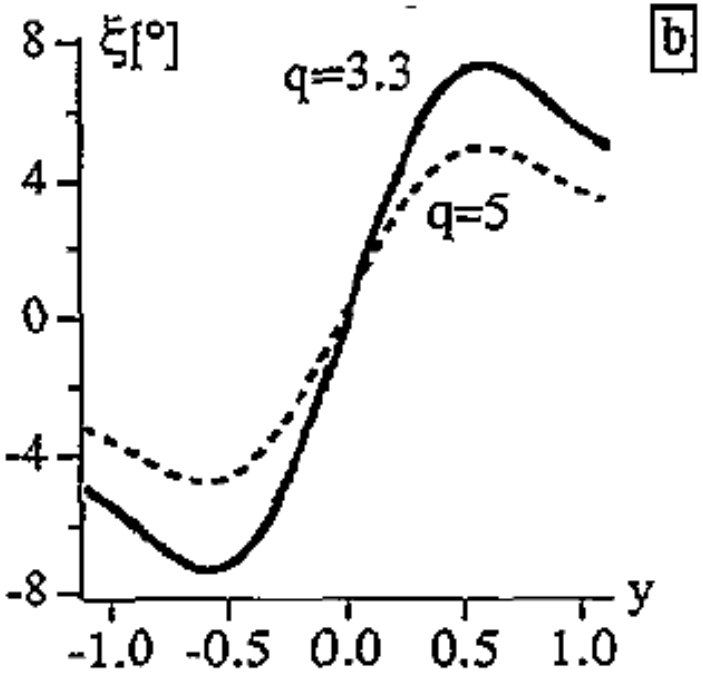


The scattering wave vector is defined by instrument geometry.
The scattering wave vector resolution is good.
The scattering localization is poor.

# Plasma microwave cutoff and resonances

Plasma refractive index: $\vec{E}_i \| \vec{B}$ $n_O = \sqrt{1 - \frac{\omega_p^2}{\omega_i^2}}$ $\vec{E}_i \perp \vec{B}$ $n_X = \sqrt{1 - \frac{\omega_p^2 (1 - \omega_p^2/\omega_i^2)}{\omega_i^2 - \omega_p^2 - \omega_{ce}^2}}$

O mode cutoff frequency: $\omega_{Oc} = \omega_p$ $n_{Oc} = \omega_i^2 \frac{m_e \epsilon_0}{q_e^2}$

X mode cutoff frequencies: $\omega_{Xh} = \frac{1}{2}\left(\omega_{ce} + \sqrt{\omega_{ce}^2 + 4\omega_p^2}\right)$ $\omega_{Xb} = \frac{1}{2}\left(\sqrt{\omega_{ce}^2 + 4\omega_p^2} - \omega_{ce}\right)$

X mode resonance frequency: $\omega_{Xr} = \sqrt{\omega_p^2 - \omega_{ce}^2}$

Reflectometry: radar principle
Cutoff surface reflection
Direct incidence on plasma

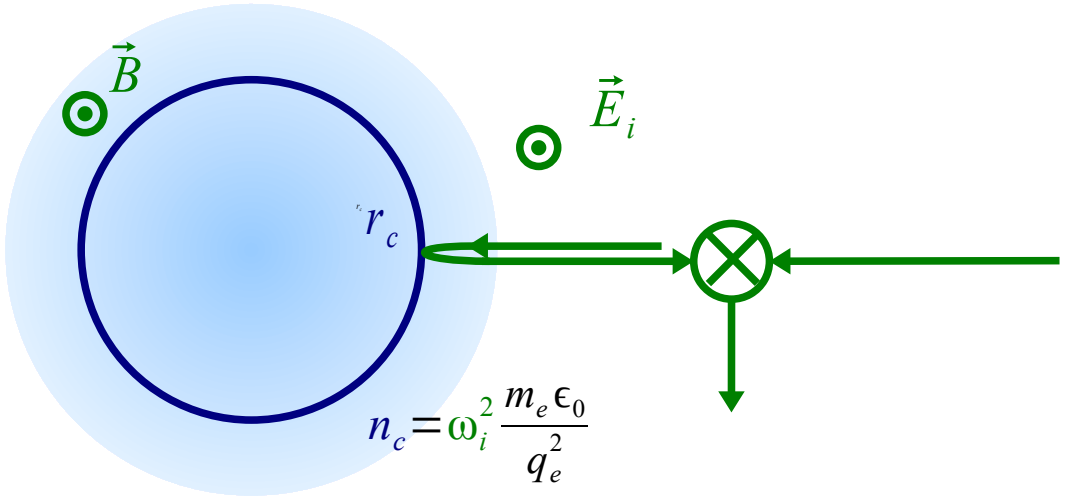


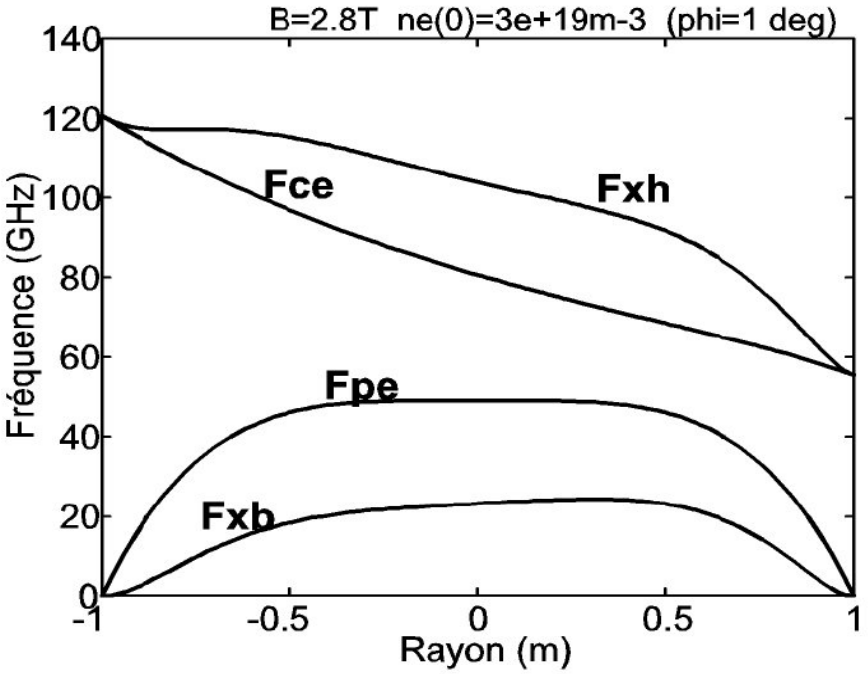

# Collective Microwave Doppler Back-Scattering

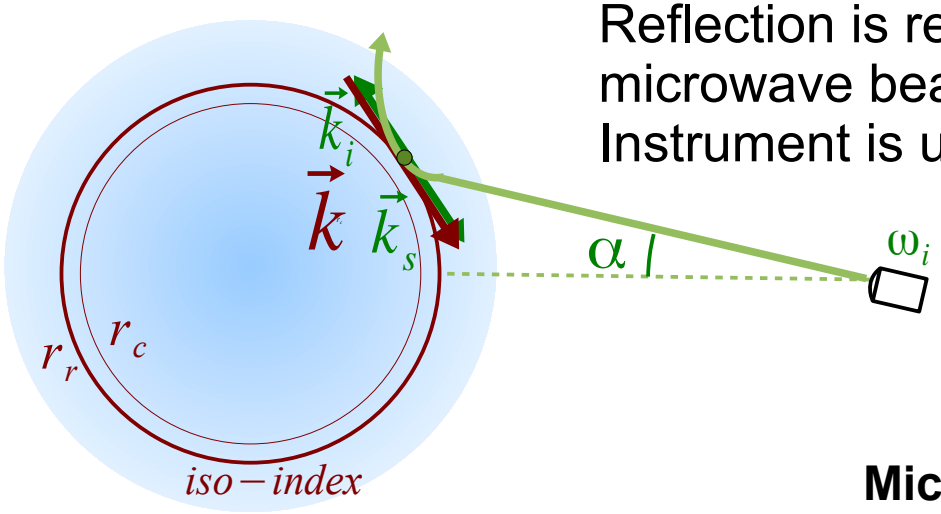


Reflection is replaced with Back-Scattering when the microwave beam is tilted from plasma direct incidence : Instrument is usually called the "Doppler Reflectometry"

$$\vec{k}_s = -\vec{k}_i$$
$$\vec{k} = -2\vec{k}_i$$

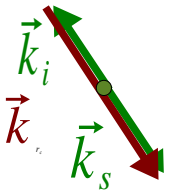


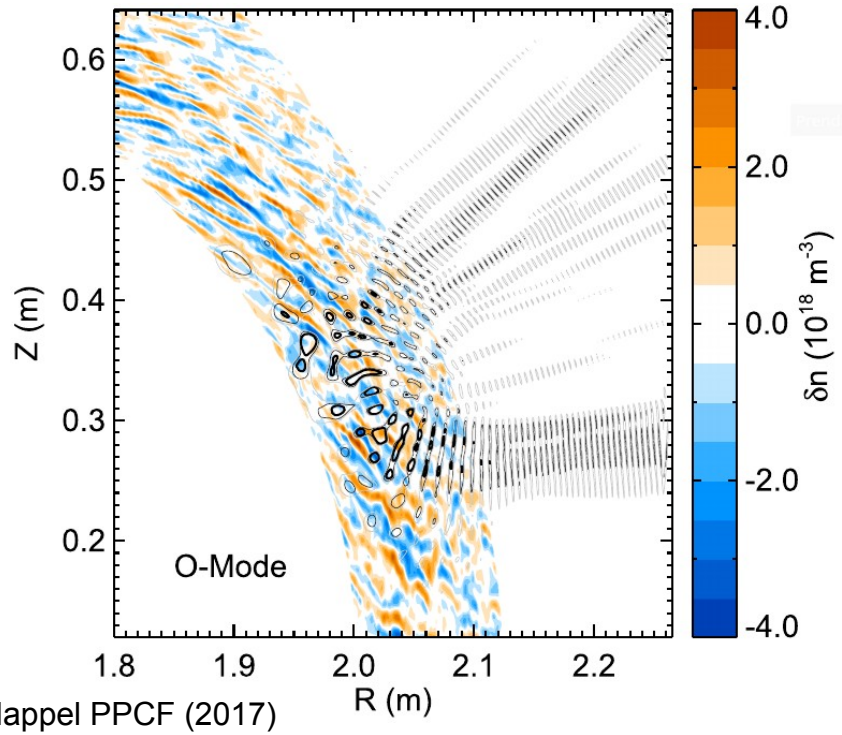


Happel PPCF (2017)

**Microwave beam back Scattering**
For these wavelengths, the beam is reflected in front of the cutoff layer.

Back scattering is **enhanced** near the reflected layer.

This enhancement is shown by beam full wave model:
- scattering volume $V_s$ is reduced
- scattering wave vector $\vec{k}$ is well defined
- scattering wave vector resolution is good.

For O mode incident waves, iso-index surfaces correspond to magnetic surfaces : the scattering wave vector is mainly **poloidal** (no radial component).

# Collective Doppler Back-Scattering

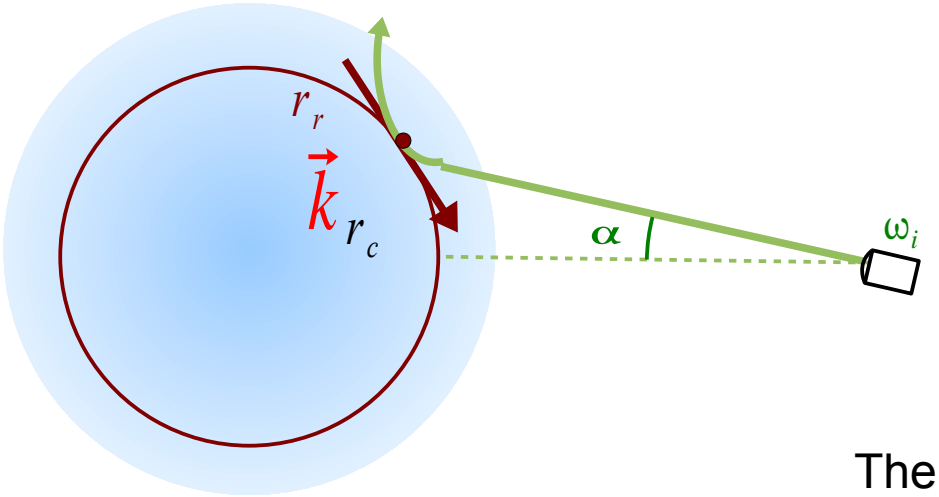


$$\vec{k} = -2\vec{k}_i$$

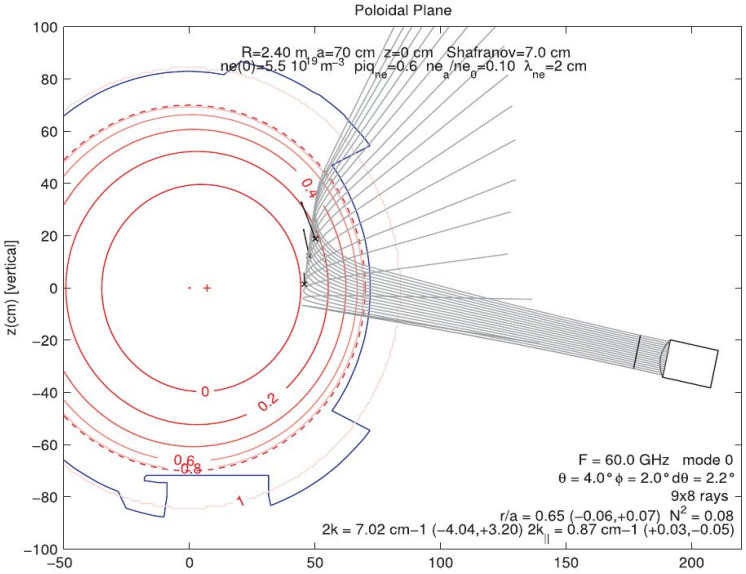


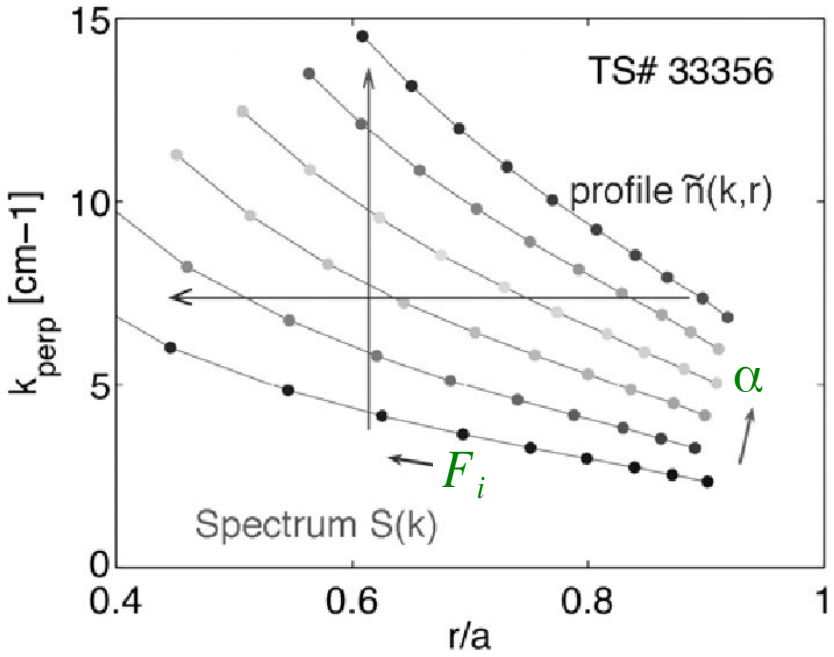


Honoré Nucl.Fus. (2006)

The microwave **refractive index** varies along the beam:

$$n_{OX}: \sim 1\,(air) \rightarrow \sim 0\,(near\ cutoff)$$

**3D Beam tracing** (WKB approximation) using plasma equilibrium and density profile is needed to determine:

$$k_i = n_{OX}\, k_{i0} = n_{OX}\, \omega_i / C$$

- the **scattering wave vector** $\vec{k}$ at the **reflection position** $r_r$
- the **beam divergence** (and so the k resolution)
- the condition $\vec{k} \perp \vec{B}$

The scattering wave vector $\vec{k}$ and position $r_r$ depend on:

- the microwave **source frequency** $\omega_i$
- the antenna **tilt angle** from direct plasma incidence $\alpha$

Different measurements allows to obtain :

- the **wave number spectra**
- and the density fluctuation and **poloidal velocity profiles**.

# Microwave Back-Scattering in Tore Supra / WEST

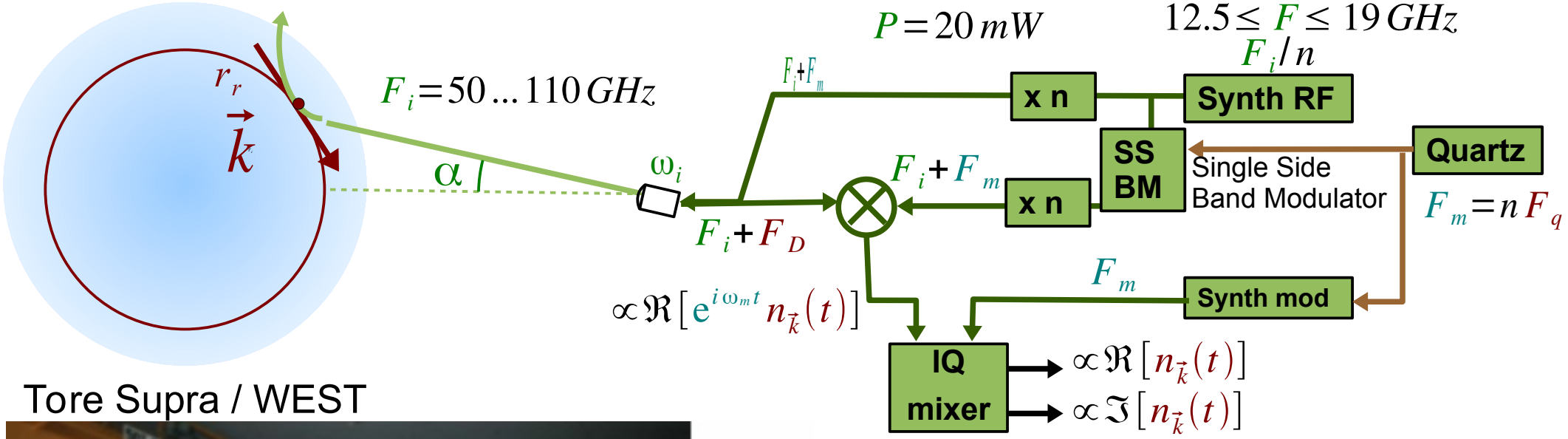


Tore Supra / WEST

Hennequin et al., Rev. Sc. Instr. (2004)

$2 \le \alpha \le 12°$

O mode, V Band:

$50 \le F_i \le 75\,GHz$

X mode, W Band:

$75 \le F_i \le 110\,GHz$

Typical :

$0{,}2 \le \lambda \le 2\,cm$

$0.8 \le \frac{r_r}{a} \le 1.05$

$0{,}3 \le \lambda \le 3\,cm$

$0.5 \le \frac{r_r}{a} \le 0.9$

# Fixed Frequency Fluctuation Reflectometry : scattering effect

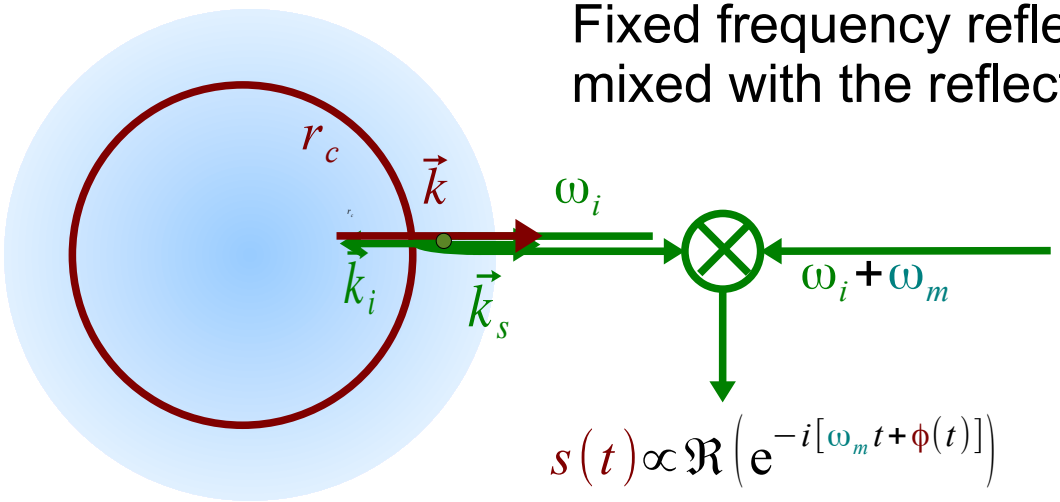


Fixed frequency reflectometry has also a scattering part mixed with the reflected signal inside the received signal

**Back-scattering** appear near the cutoff:
- scattering vector is perpendicular to the iso-index surfaces (radial for O mode)
- full wave simulations show mainly small radial wave numbers contribute.

$$k_{rn} \sim 1\, cm^{-1}$$

Reflectometry **phase fluctuations are proportional to density fluctuations** near the reflection layer.
The simplest model :

$$\tilde{\phi} = \sqrt{\frac{\pi k_i^2 L_n}{k_{rn}}} \frac{\tilde{n}}{n}$$

$L_n$ : density gradient length near the cutoff layer.
Fluctuation reflectometry is based on Thomson Scattering but with no $\vec{k}$ selection.

# Ultra Fast Sweep Reflectometry

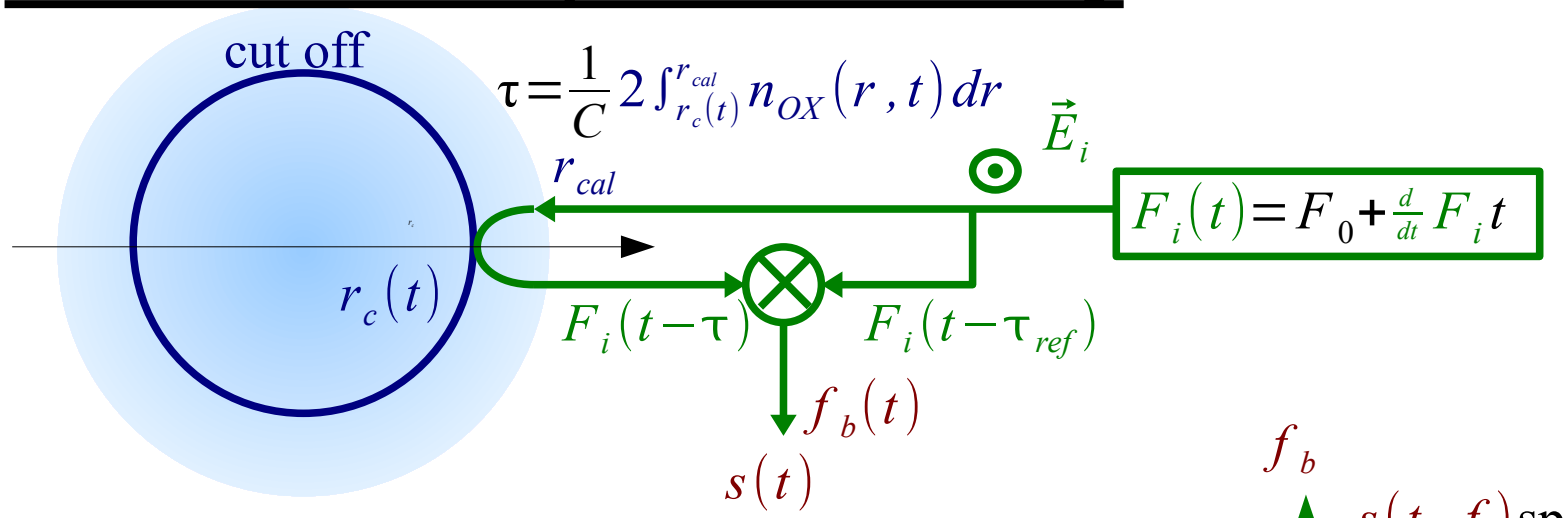


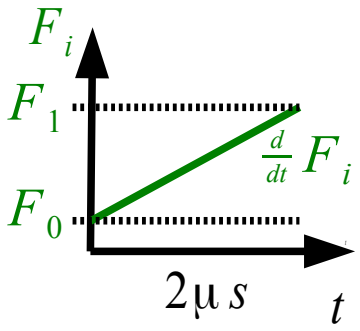


The beating frequency depends on the wave time of flight:

$$f_b(t) = \frac{d}{dt} F_i(\tau - \tau_{ref}) = f_{b\,cal} + \frac{\frac{d}{dt} F_i}{C} 2 \int_{r_c(t)}^{r_{cal}} n_{OX}(r,t)\, dr$$

$$\int_{r_c(t)}^{r_{max}} n_{OX}(r,t)\, dr \sim r_{cal} - r_c(t) \qquad \left(n_{OX}(r,t) \sim 1\right)$$

$$f_b(t) = f_{b\,cal} + \frac{\frac{d}{dt} F_i}{C} 2\left[r_{cal} - r_c(t)\right]$$

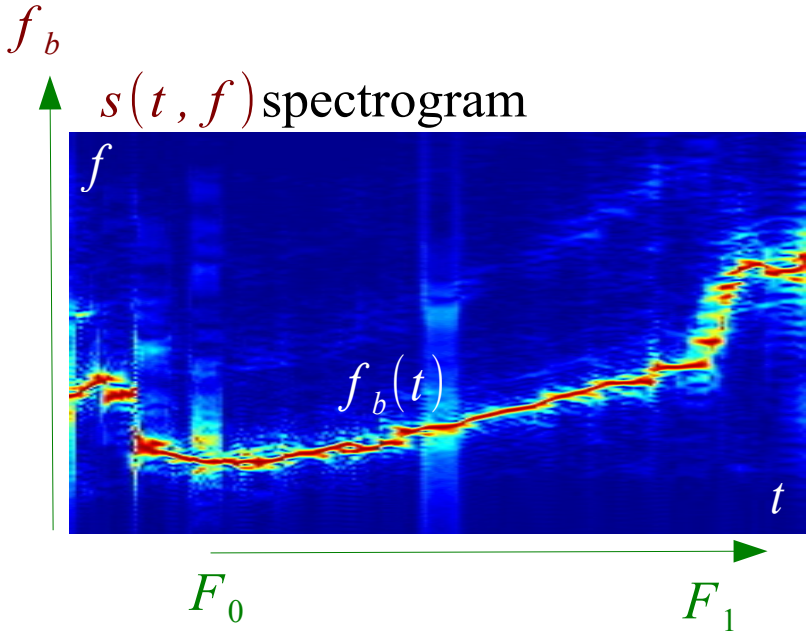


At each time along the frequency sweep ($F_i(t)$)

From the signal spectrogram you get $f_b(t)$

From the time of flight you deduce $r_c(t)$

$r_c(t)$ is the reflection position for the critical density $n_{cr}(t) = 4\pi^2 F_i(t)^2 \frac{m_e \epsilon_0}{q_e^2}$

Ultra Fast Sweep Reflectometry is used to determine density profiles $n(r)$ on very short delays.

# Sweep Reflectometry phase fluctuations: propagation effect

Ultra fast Sweep Reflectometry signal phase fluctuations are mainly linked to the effect of density fluctuations on the wave propagation.

The refractive index is modified by density fluctuations:

$$n_{OX}(r)^2 = n_{OX0}(r)^2 + \alpha_{XO}(r)\, n_{e1}(r)$$

The ratio between the density and the refractive index is direct for O mode propagation

$$\alpha_O^2 = \frac{-1}{n_{cr}}$$

The fluctuations perturbs the wave propagation (Helmholtz equation):

0th order: $$\left[\frac{d^2}{dr^2} + k_i^2\, n_{OX0}(r)^2\right] E_{i0}(r) = 0$$

1st order: $$\left[\frac{d^2}{dr^2} + k_i^2\, n_{OX0}(r)^2\right] E_{i1}(r) = -\alpha_{OX}(r)\, n_{e1}(r)\, k_i^2\, E_{i0}(r)$$

The Green function solution includes the phase correction:

$$\tan\Delta\phi = -2\, k_i^2\, W^{-1} \int \alpha_{OX}(r)\, n_{e1}(r)\, A_i^2(r)\, dr$$

$A_i(r), B_i(r)$ : Airy functions $\left(\frac{d^2}{dr^2} + r\right) f = 0$

$W = \frac{1}{\pi}$ : Airy function Wrońskian

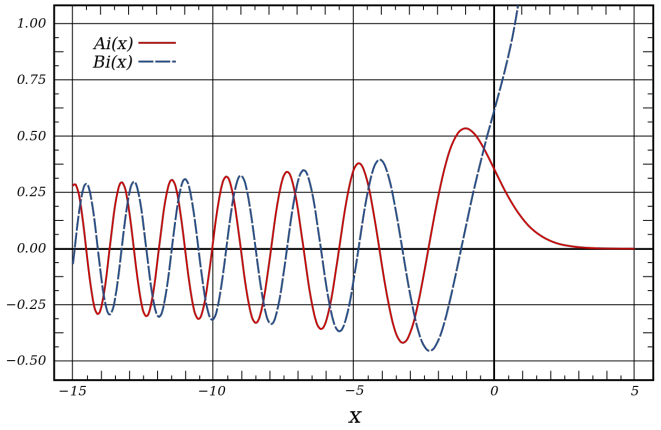

# Collective Thomson Scattering

# Confinement and micro-turbulence

$\tau_E^{-1}$

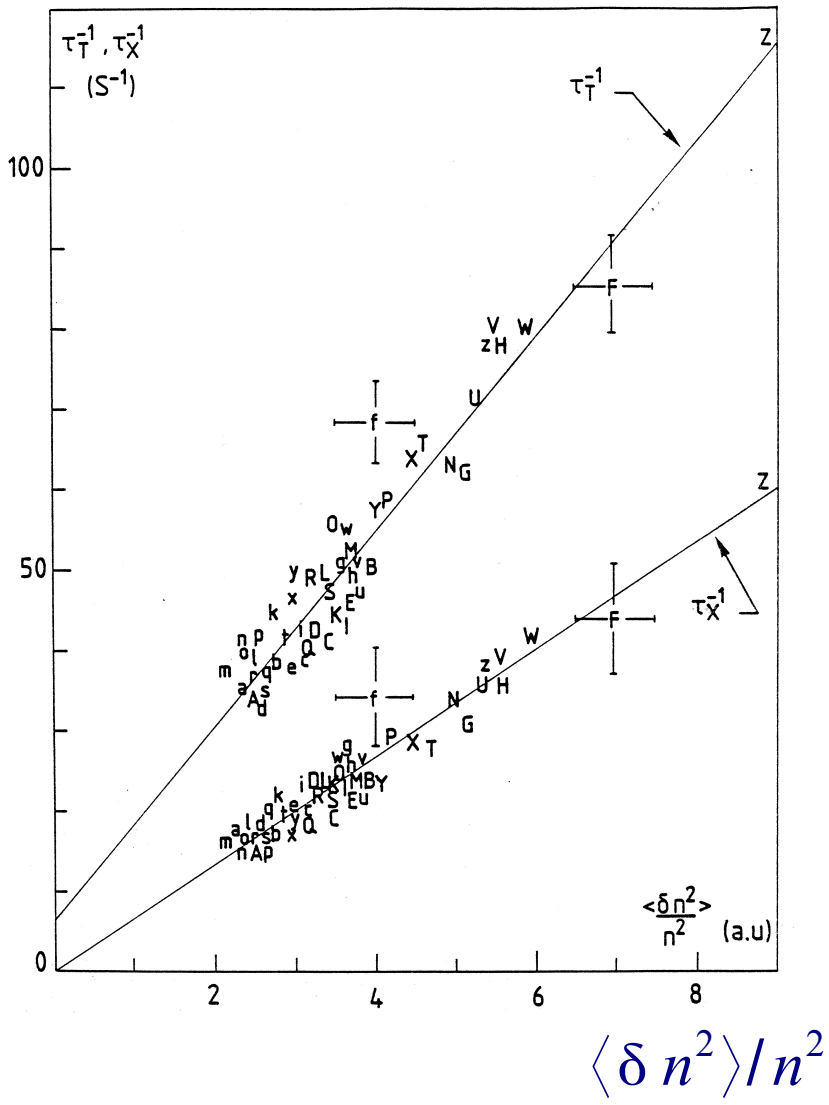


Application of laser collective Thomson forward scattering on TFR tokamak

**Collective scattering** showed the confinement loss is correlated to the density fluctuation level.

$\tau_T$ : transport confinement time

$\tau_\chi$ : transport confinement time taking into account sawtooth losses

TFR group et al., Nucl. Fus. (1986)

# Ultra Fast Sweep Reflectometry on JET

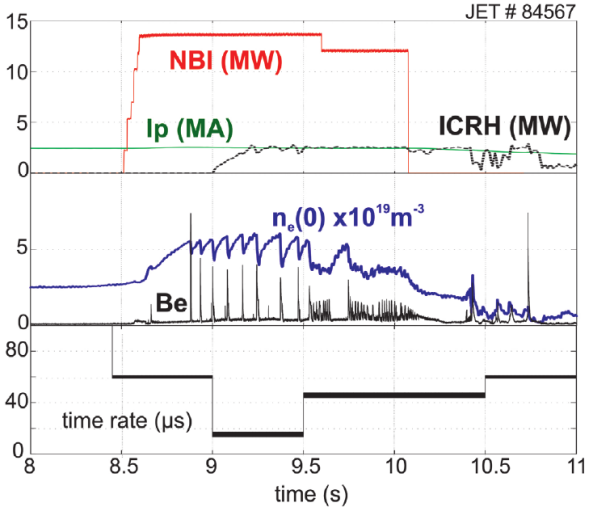


Density fluctuation measurements
with an Ultra Fast Sweep Reflectometer on JET Tokamak

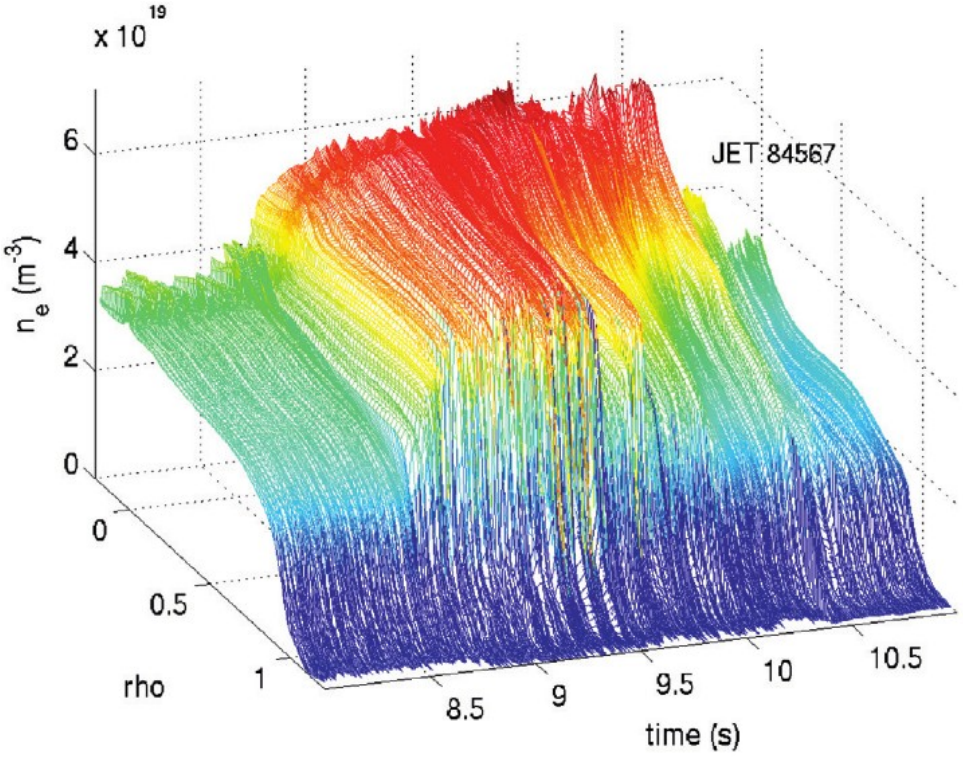


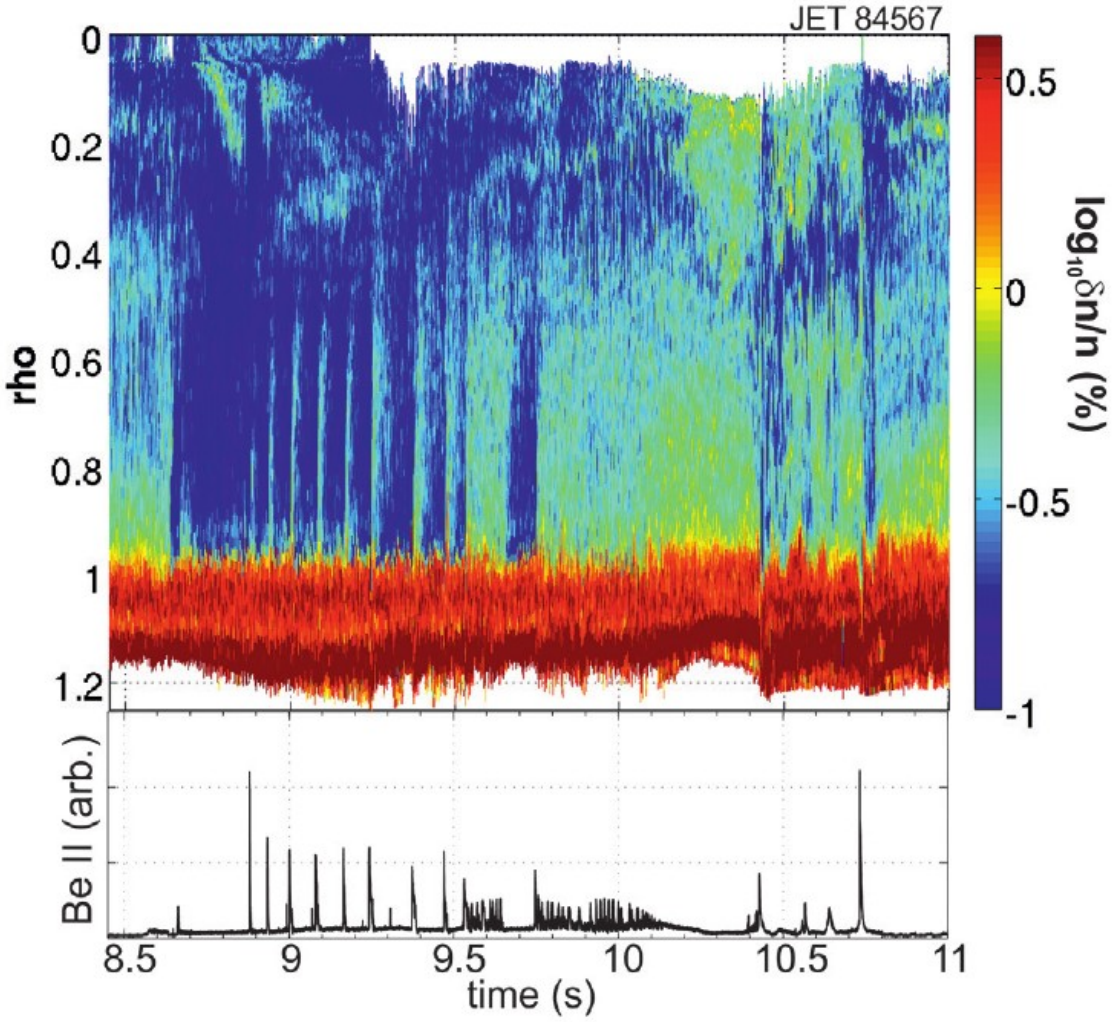


F; Clairet, Nucl. Fus. (2016)

# Density fluctuation level across the plasma on Tore Supra

Comparison between density fluctuation level measured by fixed frequency reflectometer (DREFLUC) and frequency sweep reflectometer (DREFLEC).

Density fluctuations are low in the core plasma and increase in direction of the edge.

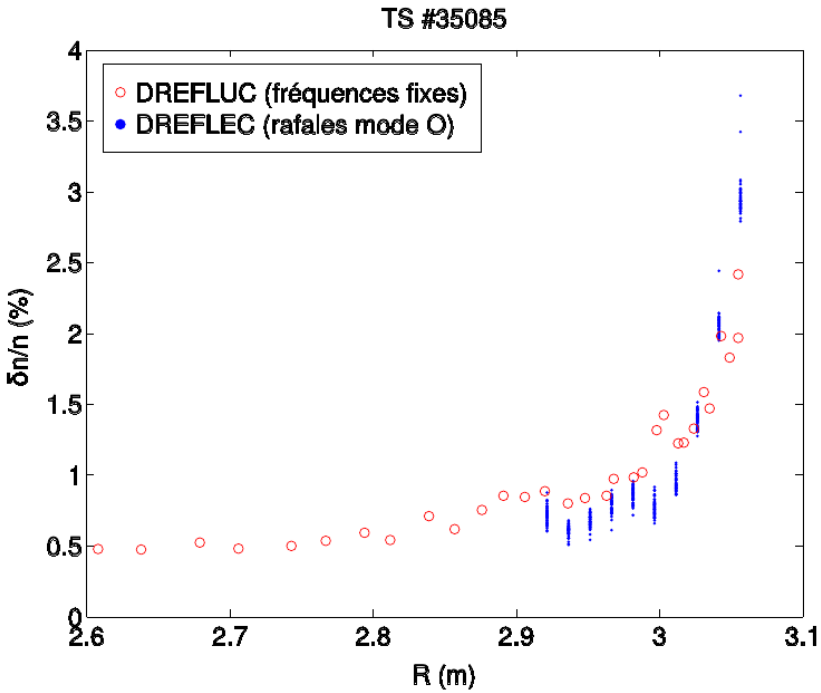


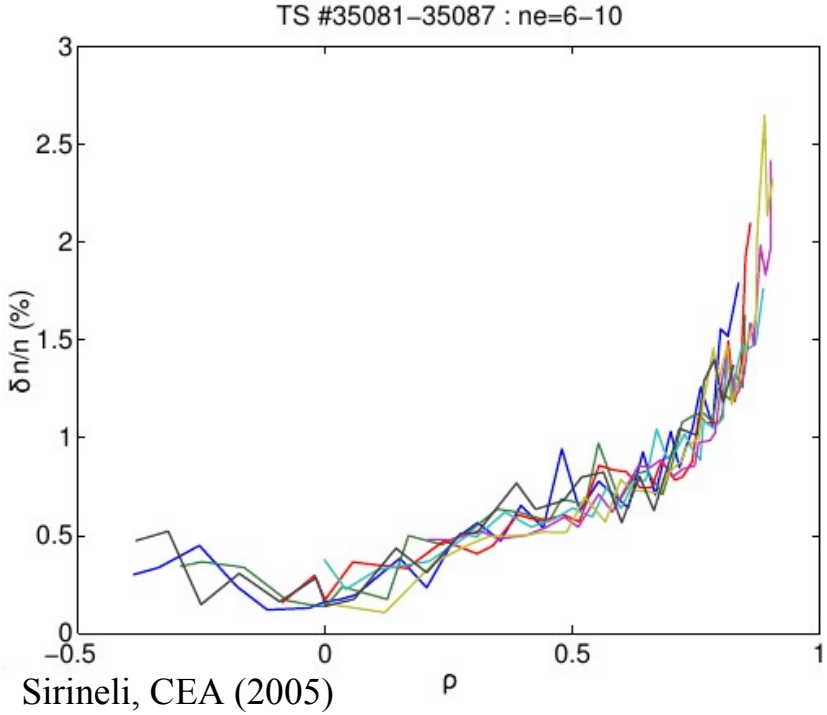


Sirineli, CEA (2005)

Density relative fluctuation level does not depend on the density level :
Saturated Ohmic Confinement regime is reached.

# 2D Turbulence : energy and enstrophy transfer across scales

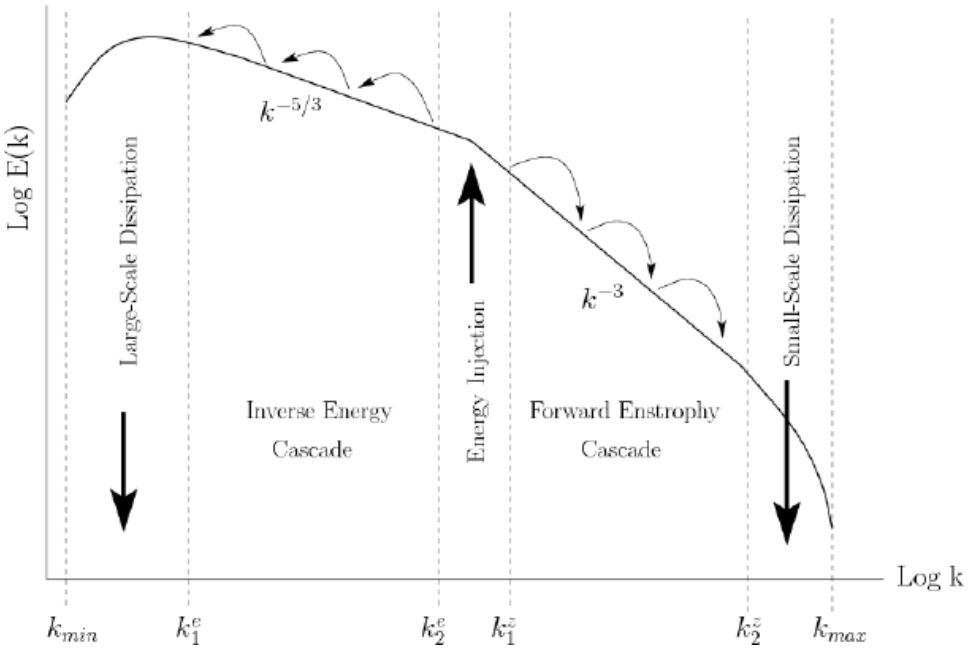


M. Farazmand et al. JFM (2011)

2D turbulence, R. Kraichnan (1967):

The energy is injected at a specific scale.
In 2D, it is shown the enstrophy (vorticity intensity) is conserved from the production scale to smaller scales at constant rate, until the scale where it is dissipated.
In this cascade the energy is not conserved: the energy goes from the production scale to larger scales at constant rate until it is dissipated.

O. Gürcan, PPCF (2010)
Derivation of a shell model:
the model describes drift wave isotropic turbulence.
Length are normalized to $\rho_s$.

$$\langle|\tilde{n}_k|^2\rangle \sim \langle|\tilde{\Phi}_k|^2\rangle \sim \frac{k^{-3}}{(1+k^2)^2}\mathrm{e}^{-\lambda k}$$

# Scattering signal wave number spectra

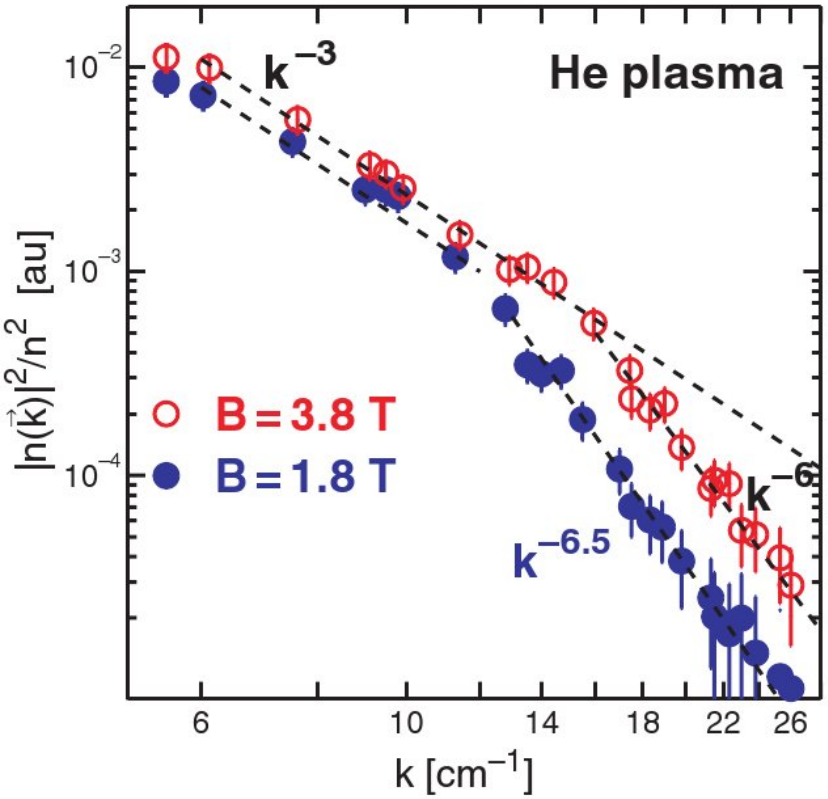


Laser collective Thomson scattering
Static form factor

Scattering signal wave number spectra show power laws for different wave number range.

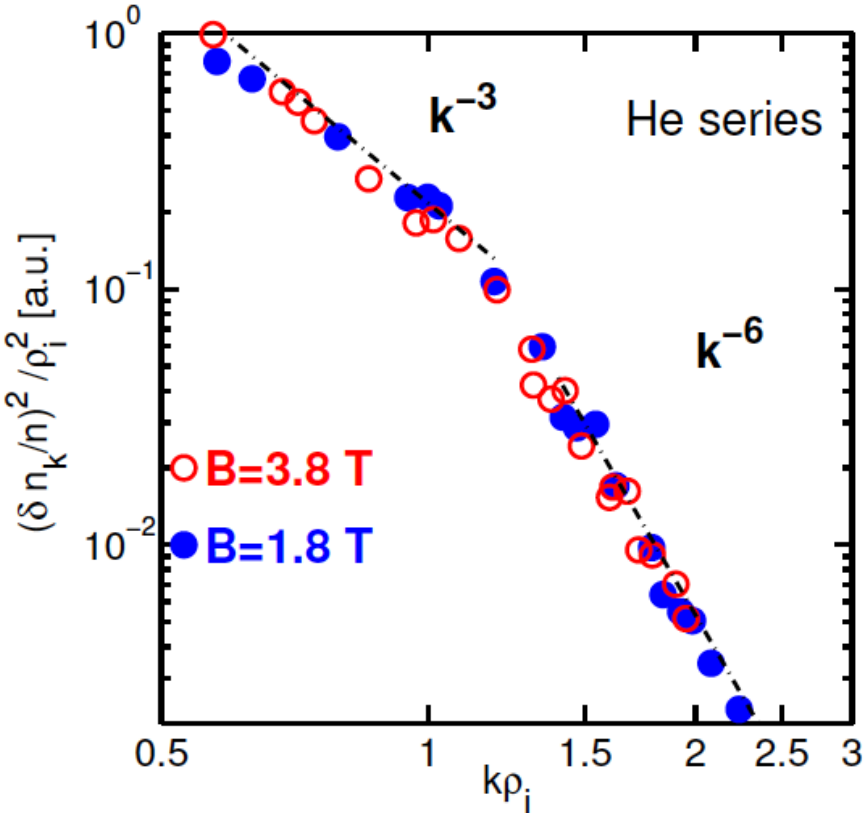


When wave number is normalized to $\rho_{ci}$, data follow the same shape.

Hennequin et al., Rev.Sc.Instr. (2004)

# Scattering signal wave number spectra

Comparison between observed wave number spectra with the shell model spectra:
the agreement is good for small scales.

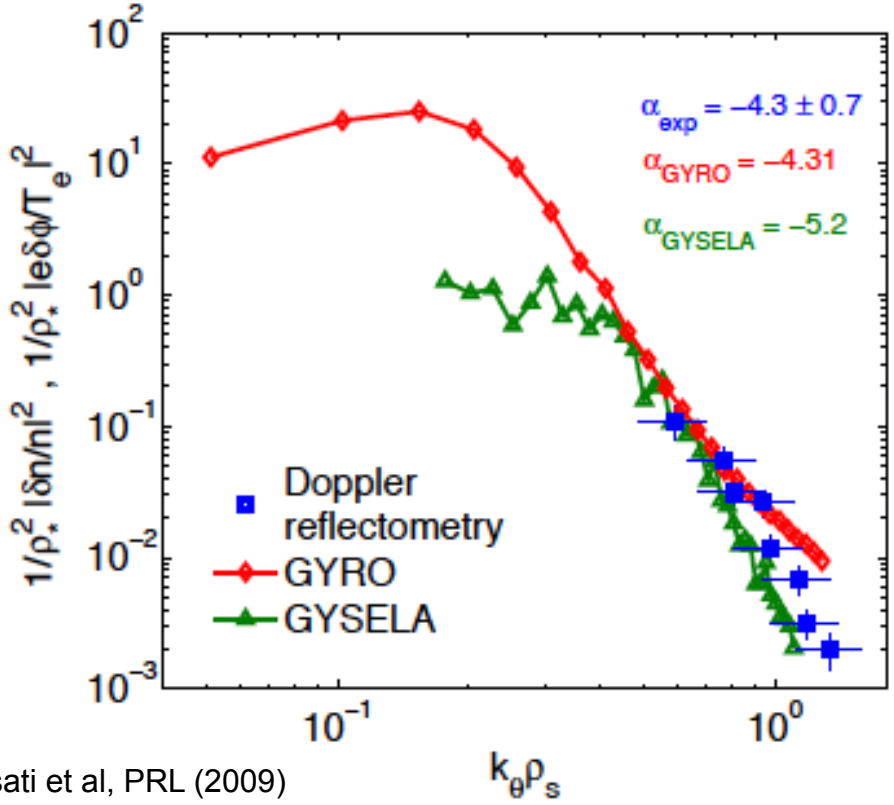


Casati et al, PRL (2009)

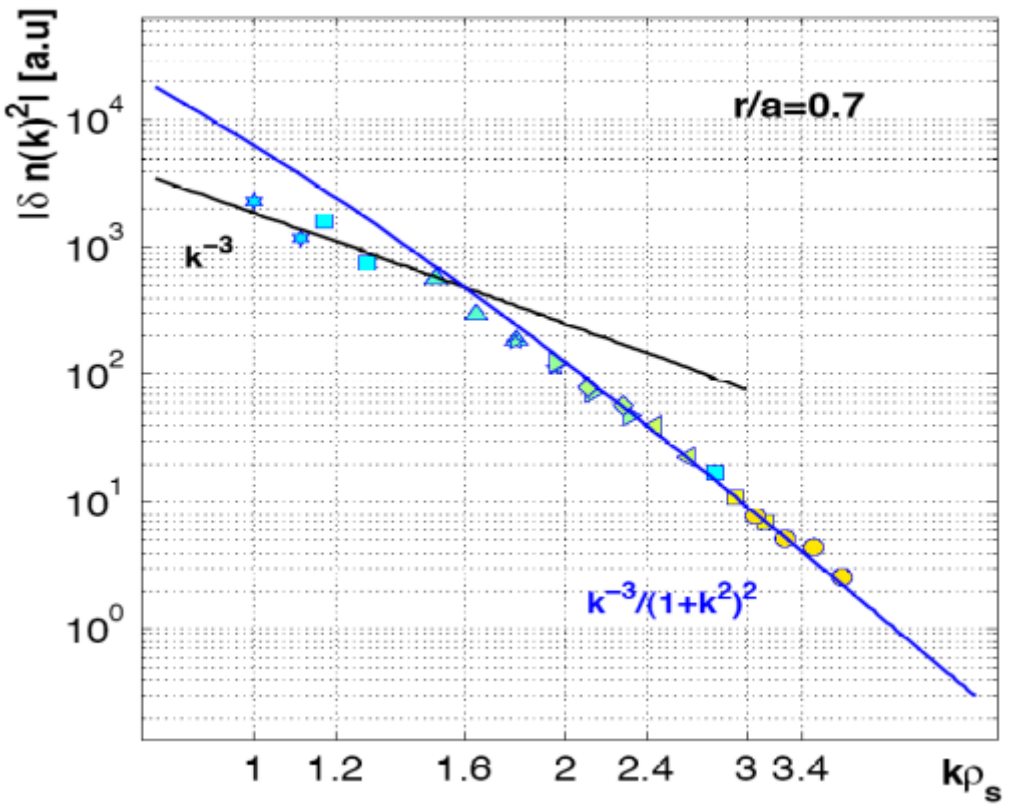


Comparison between gyrokinetic models and k spectra shows also a good trend agreement for small scales.

# Collective Scattering Doppler Frequency and Poloidal Velocity

# Poloidal velocity

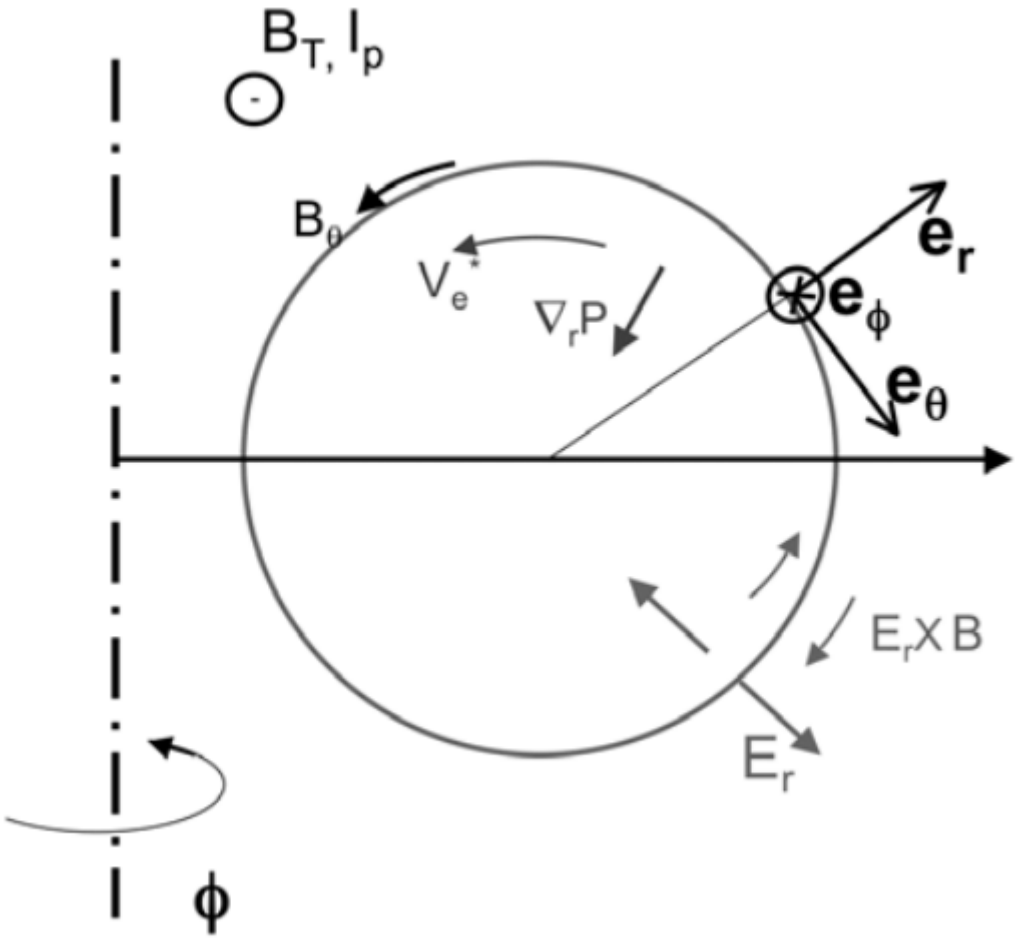


Tokamak plasma rotates in the poloidal direction :
electric potential may vary between magnetic flux surfaces : an **electric field** may appear in the radial direction.

The radial electric field might be :
- due to MHD instabilities,
- due to additional heating / current drive,
- due to magnetic ripple in the toroidal direction (due to the finite number of toroidal magnetic field coils).

This radial electric induces a **poloidal ExB drift**.

Drift turbulence might have also a poloidal **phase velocity** in the **electron diamagnetic drift** direction.

# Scattering signal Doppler frequency

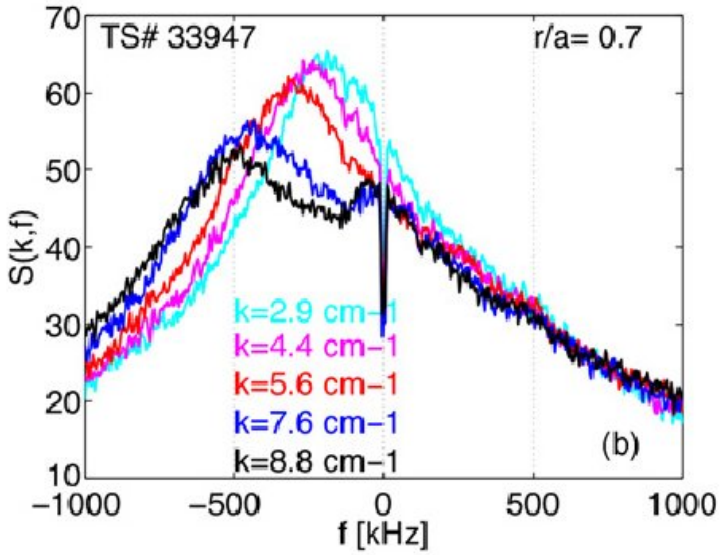


P. Hennequin et al., Nuclear Fus. (2006)

Microwave Back-Scattering:
Collective scattering frequency spectra for different wave number:
The Doppler frequency and Doppler peak width are proportional to the wave number.

$$S(\vec{k},\omega)=\frac{2\pi}{k}S(\vec{k})P_{U_{\vec{k}}}\left(\frac{-\omega}{k}\right)$$

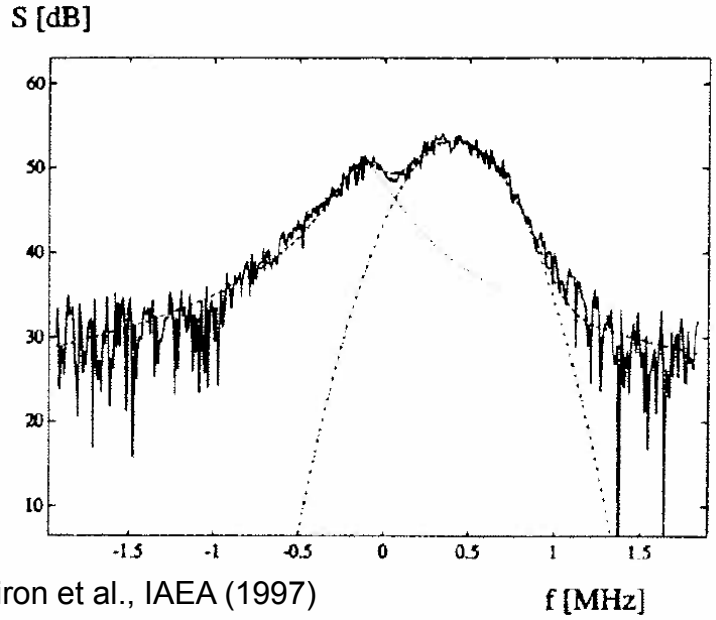


C. Laviron et al., IAEA (1997)

Laser Forward-Scattering:
because of the poor localization, 2 Doppler peaks appears for opposite poloidal velocities.

Doppler peak shapes differ:
- the negative frequency peak is larger at the base due to **diffusion**.
- The positive frequency peak has a **Gaussian** shape.

# Between Gaussian and Lorenzian shape

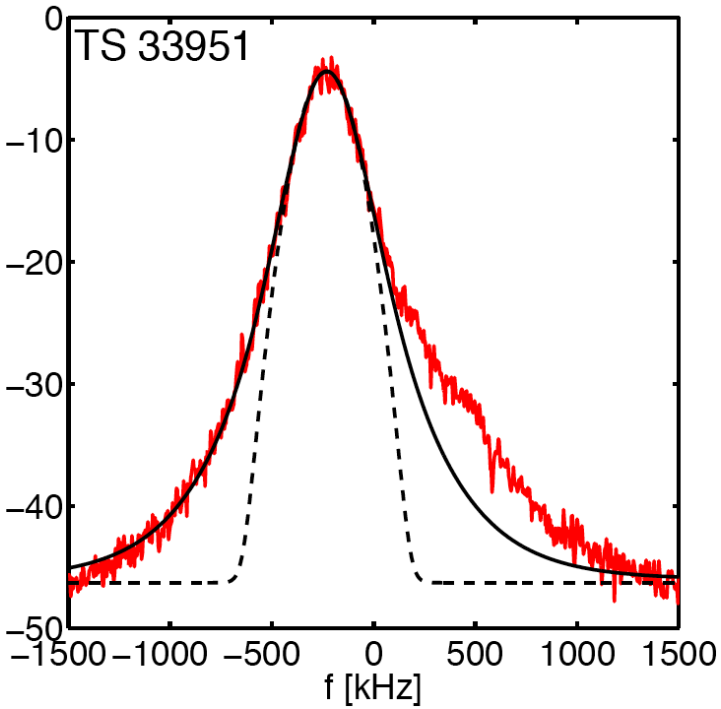


P. Hennequin, Nuclear Fus. (2006)

Microwave Back-Scattering :
the shape of the Scattering signal frequency spectrum is fitted with Gaussian and profiles, and profiles corresponding to the signal correlation with a Taylor function shape (including the diffusion effect).

The peak shape that includes the diffusion effect is very close to the scattering signal frequency spectrum.

# Scattering signal modulus and Doppler frequency

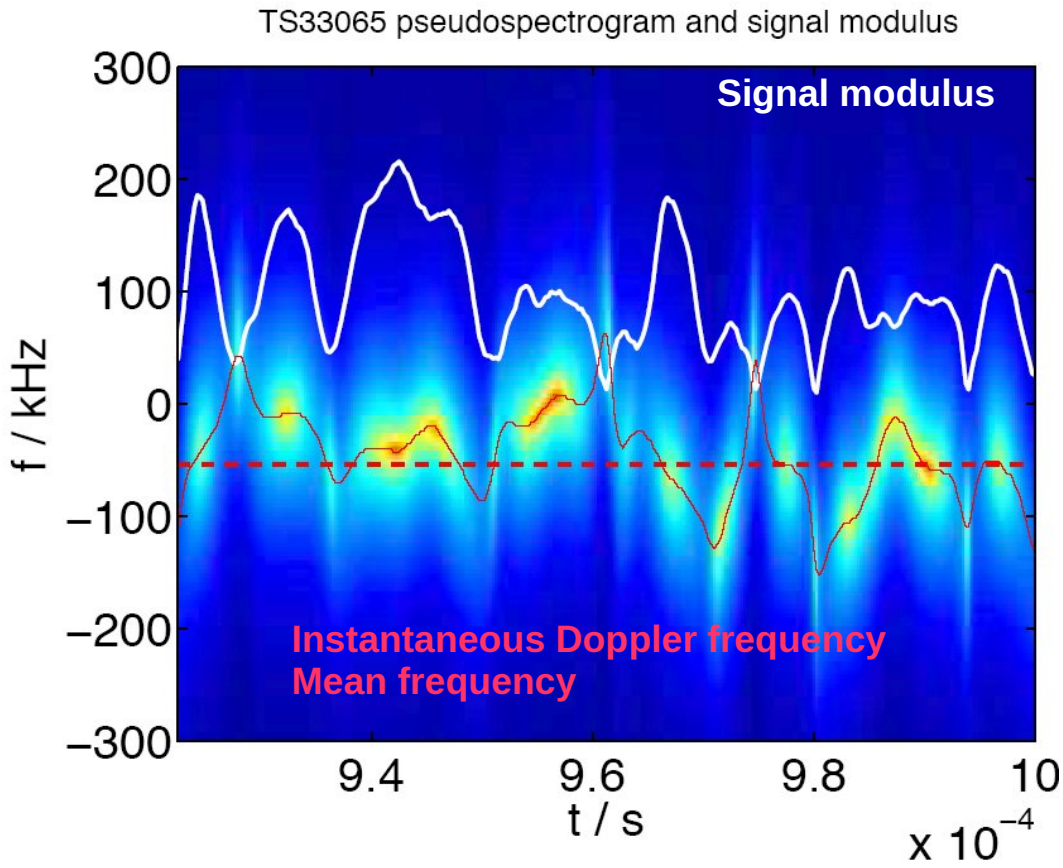


P. Hennequin

Scattering signal pseudo spectrogram and modulus :

The comparison between the modulus and signal frequency dynamics shows there is a correlation between both.

# Scattering signal Doppler velocity profile

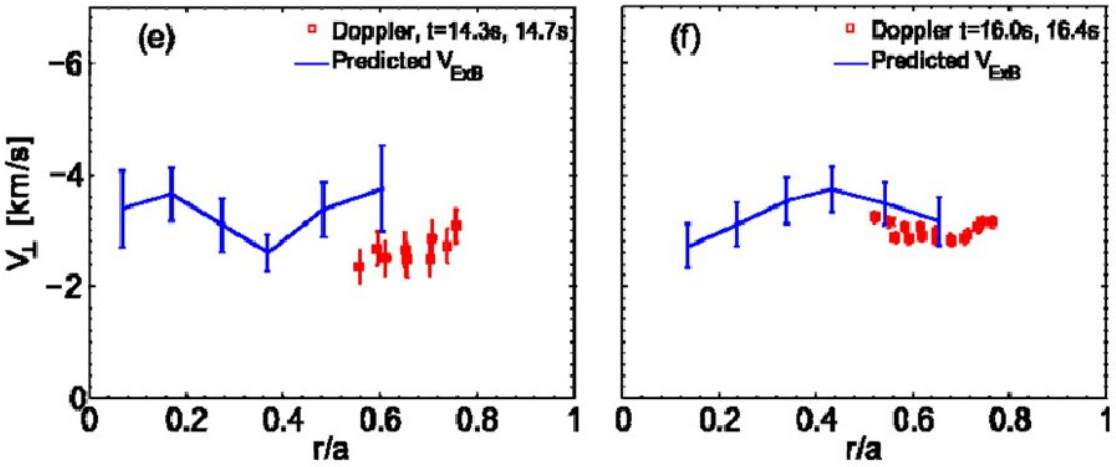


Comparison between the poloidal velocity observed with microwave collective scattering and ExB velocity evaluated with Charge exchange recombination spectroscopy (CXRS).

They are different : the collective scattering poloidal velocity should include the drift wave phase velocity.

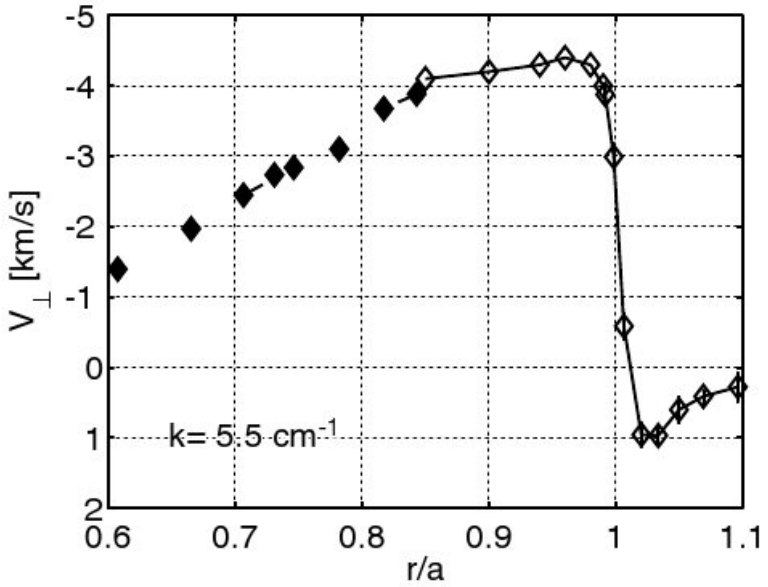


Most of the time the difference is small and not significant

Poloidal velocity profiles shows there is a poloidal velocity inversion close to the last closed flux surface.

Hennequin et al., Nucl. Fus. (2006)

# Scattering signal Doppler velocity : turbulence shear

The radial electric field induces a poloidal ExB drift varies along the radial direction.

When the electric varies rapidly, this creates a **poloidal velocity shear**.

This velocity shear has an effect on the micro-turbulence :
**Larger scale structures are distorted** by the velocity shear.

**The micro-turbulence is reduced** at the position of the shear.

Poloidal velocity shear due to steep radial electric field radial variation **reduces the transport** at this position.

Velocity shear at the edge plays an important role in the L to H mode transition.

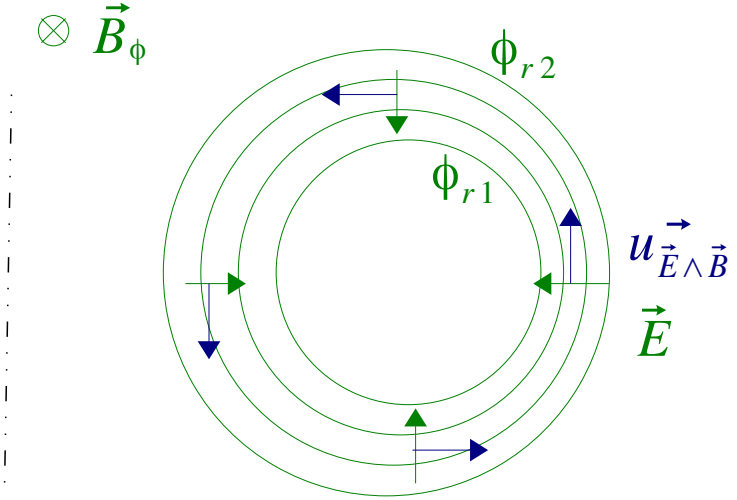


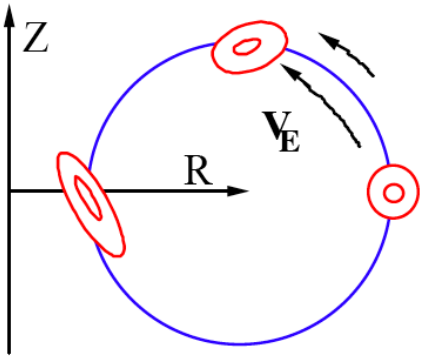


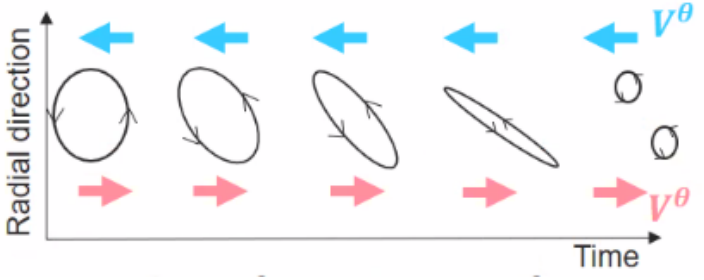

# Poloidal velocity shear and turbulence reduction effect

Radial electric field evaluated from the scattering signal frequency

**Scattering signal modulus radial correlation** (using 2 different scattering instruments).

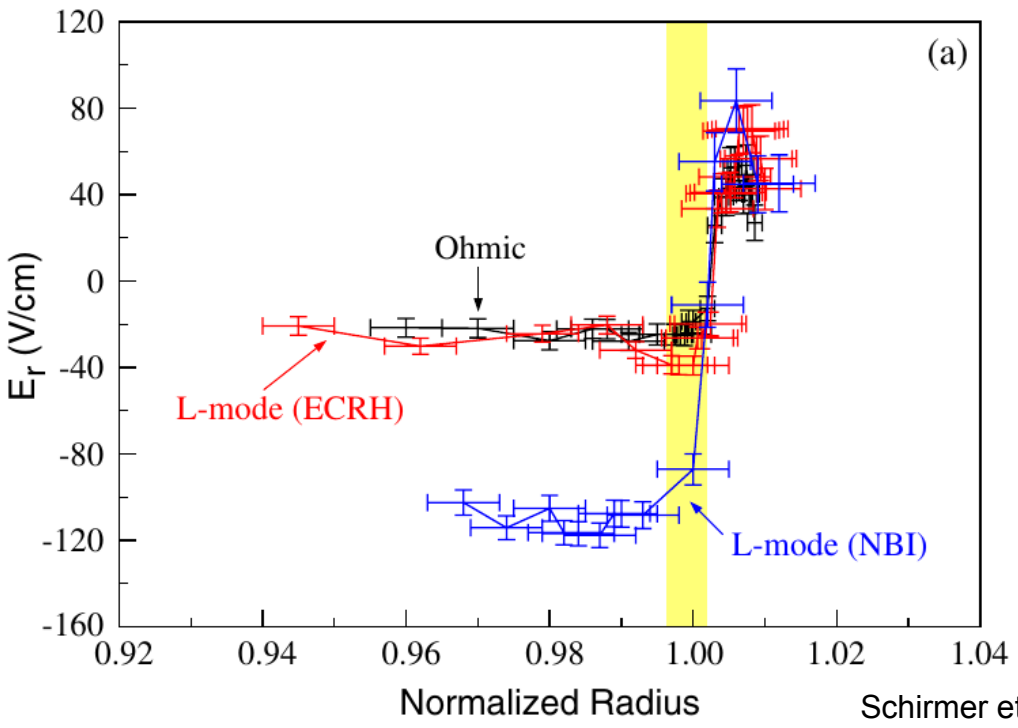


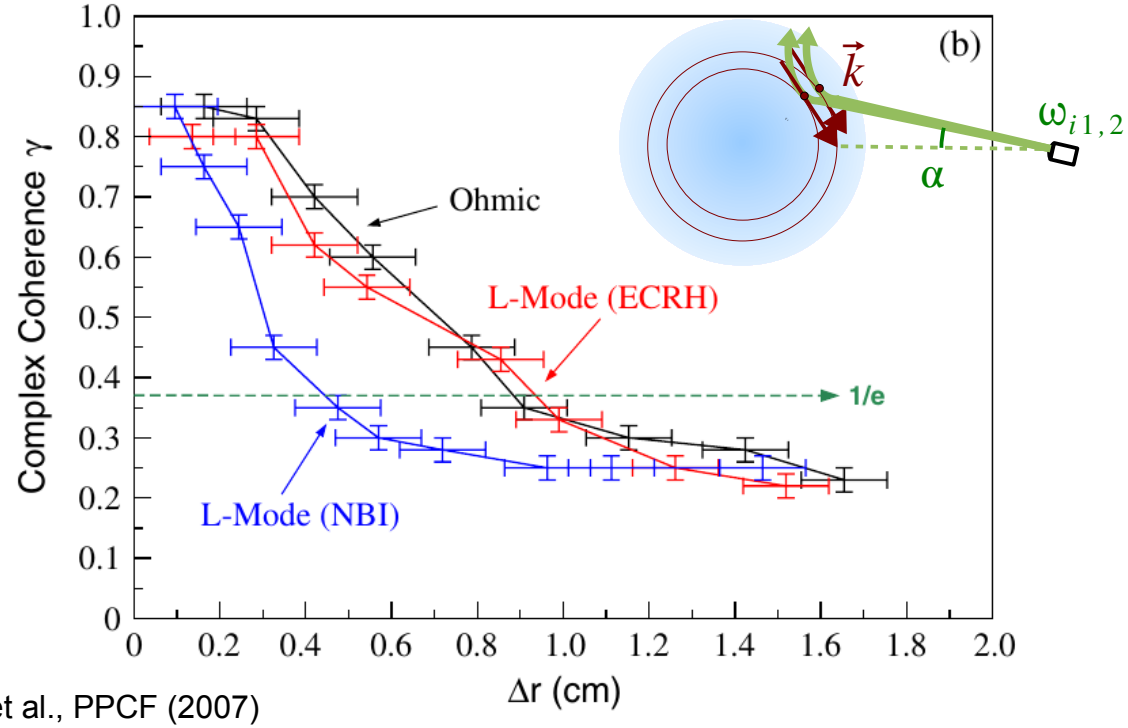


Schirmer et al., PPCF (2007)

Scattering signal modulus radial correlation shows the radial correlation length is reduced when the poloidal velocity shear is getting steeper.

# Scattering signal modulus radial Correlation

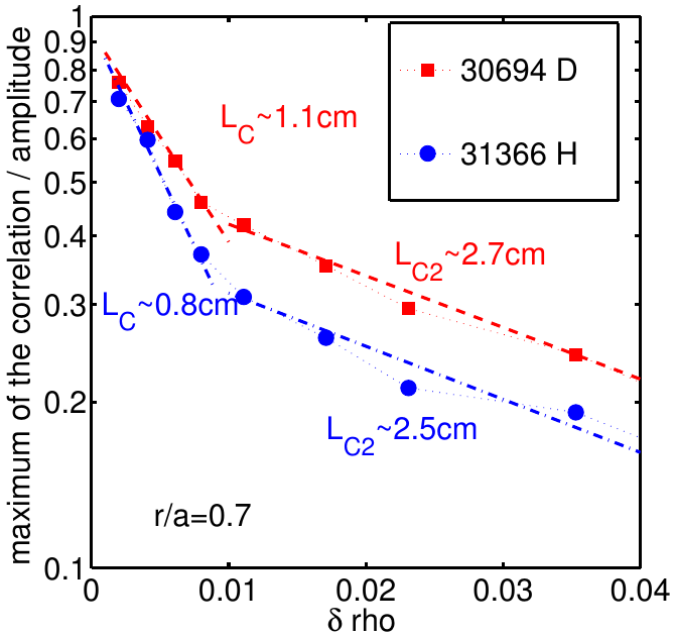


P. Hennequin et al., EPS (2015)

More detailed scattering signal modulus radial correlation analysis show there is a secondary larger radial correlation length : it might correspond to rarer larger scale transport.

# H mode : velocity shear

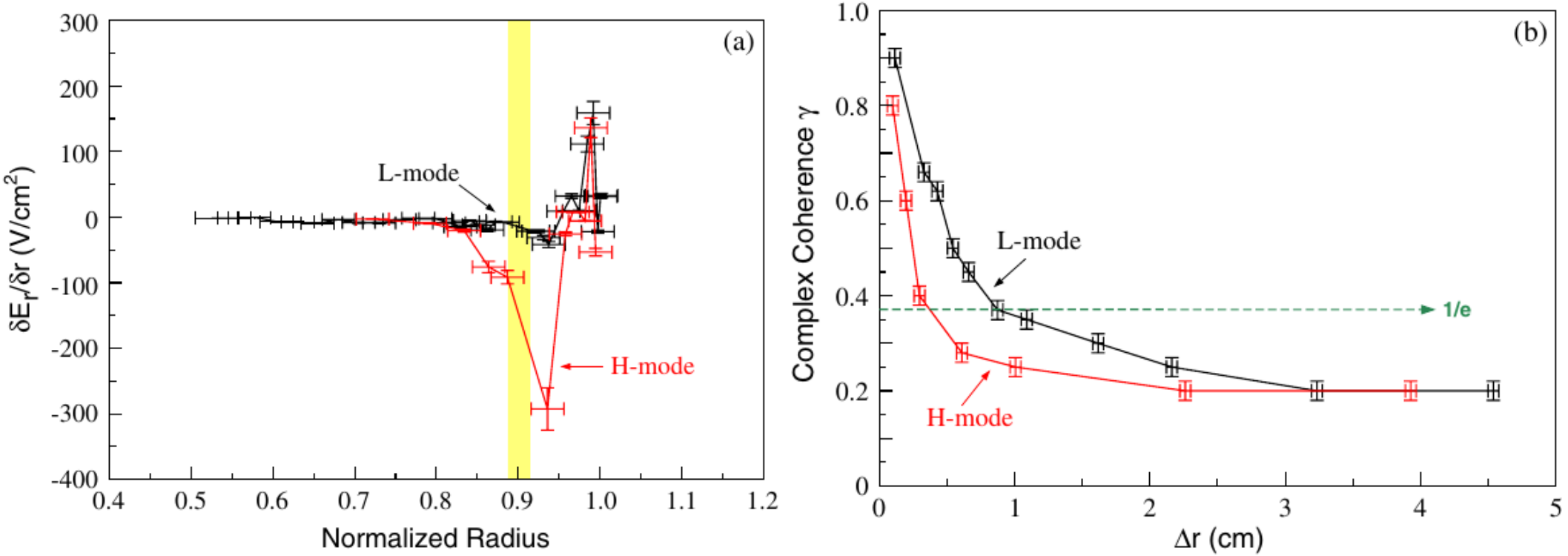


J. Schirmer et al., PPCF (2007)

After L-H transition, the ExB poloidal velocity shear is even steeper.
The radial correlation is even more reduced.
The reduced transport through this layer allows the confinement enhancement.

# H mode : ELM observation

Microwave Collective Scattering instrument observes H mode pedestal.

$\rho = r/a = 0.99$

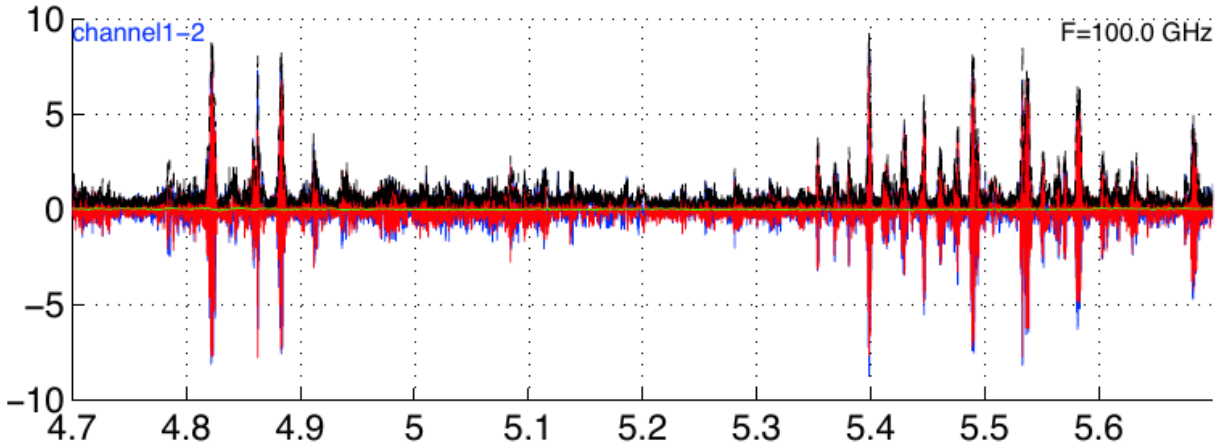


Type I ELMs

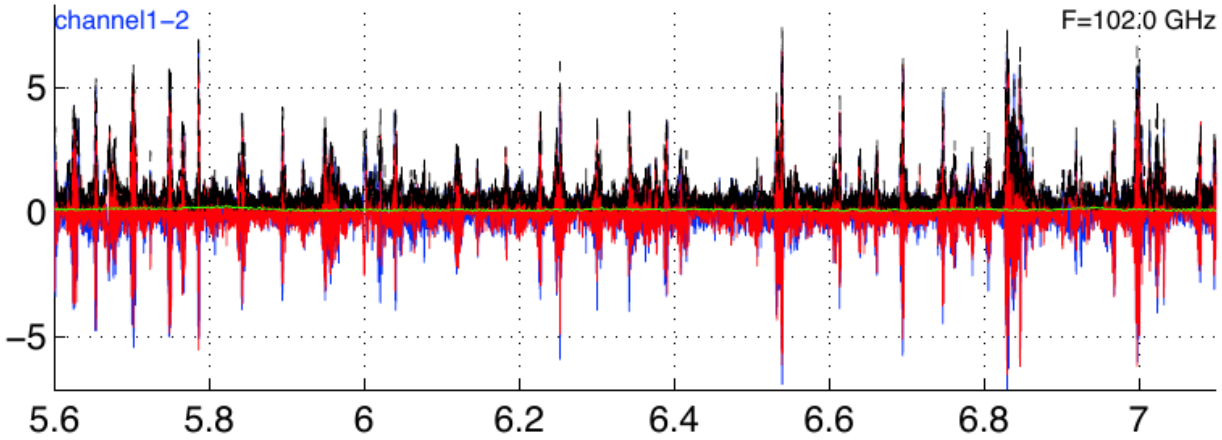


Higher frequency and smaller ELM phase

P. Hennequin et al., EPS (2017)

# Zonal Flows

Zonal flows are m=0 and n=0 modes : the electric potential is uniform on magnetic flux surfaces, but varies between surfaces. They are created by radial current.

P. Morel, M2PPF (2020)

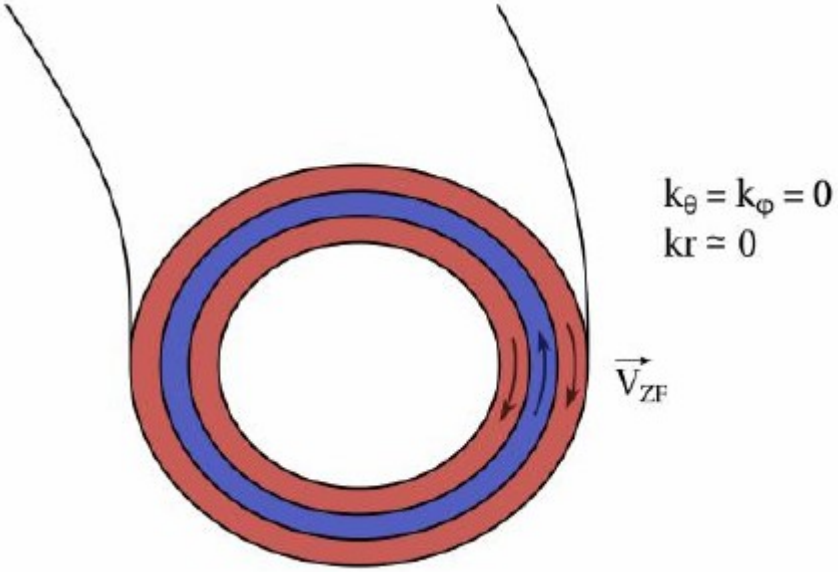


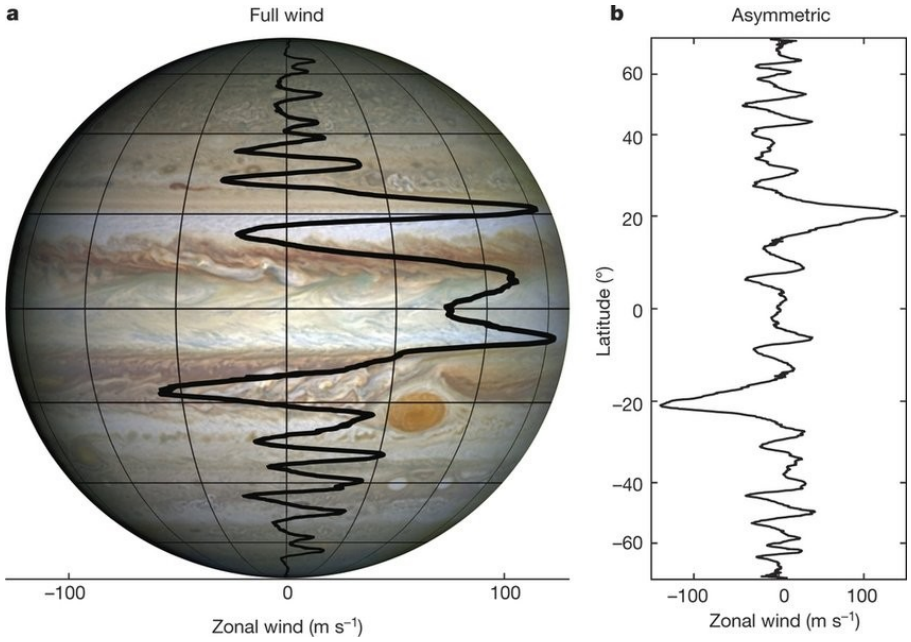


Y. Kaspi et al., Nature (2018).
Juno (2016) + Hubble (2014)

Zonal flows are observed on planetary atmospheres (Jupiter, earth)

# Zonal Flows : turbulence interaction

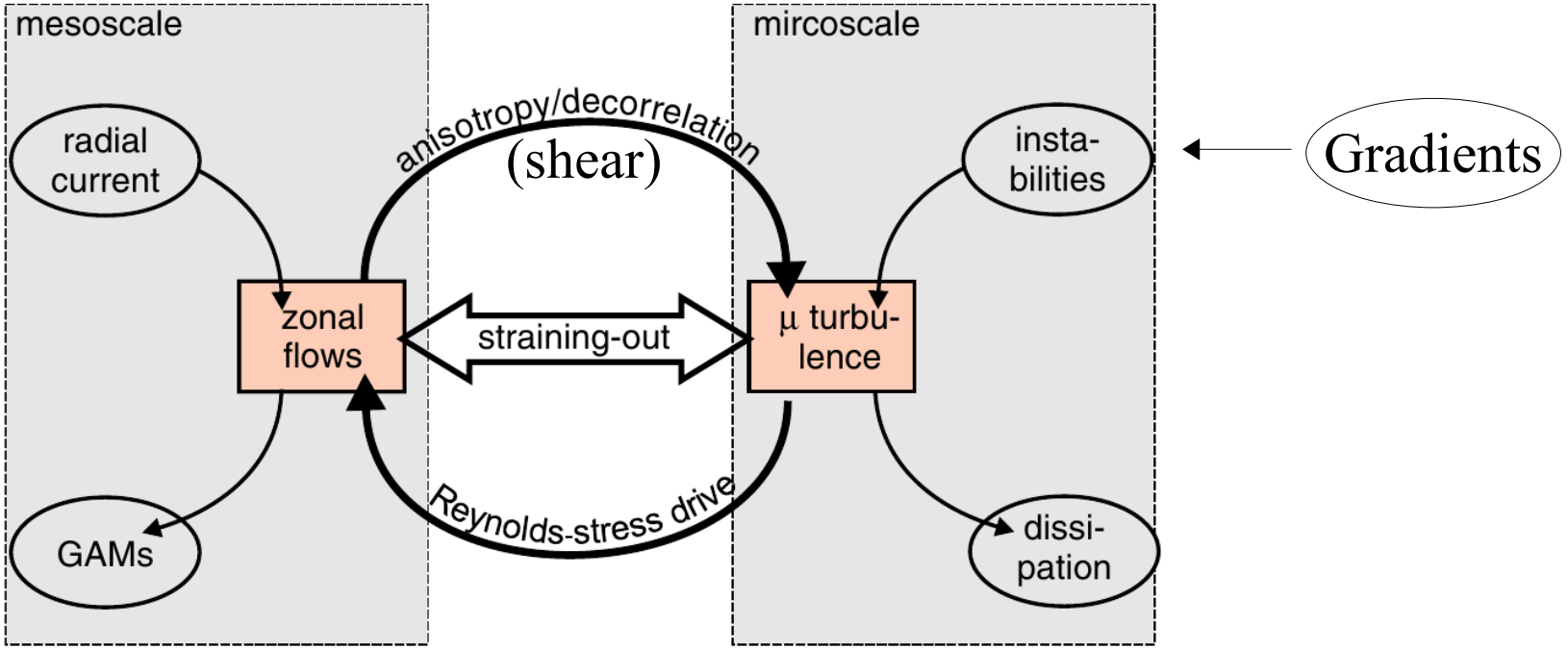


U. Stroth et al., PPCF (2011)

The zonal flows reduce the the micro-turbulence by the anisotropy and the de-correlation by shearing effect.

The micro-turbulence has a reciprocal effect on the zonal flows : they drive them through the Reynolds stress.

# Geodesic Acoustic Modes

Geodesic acoustic modes (GAMs) are oscillating zonal flows (m = n = 0) for a localized radial zone. They are low frequency (a few kHz) in the Er × B poloidal plasma flow.
The flow perturbation couples, via the geodesic curvature of the magnetic field, to an axisymmetric pressure mode (m = ±1, n = 0) to create an mainly electrostatic eigenmode oscillation.
The GAMs, like zonal flows, interact with the plasma micro-turbulence.

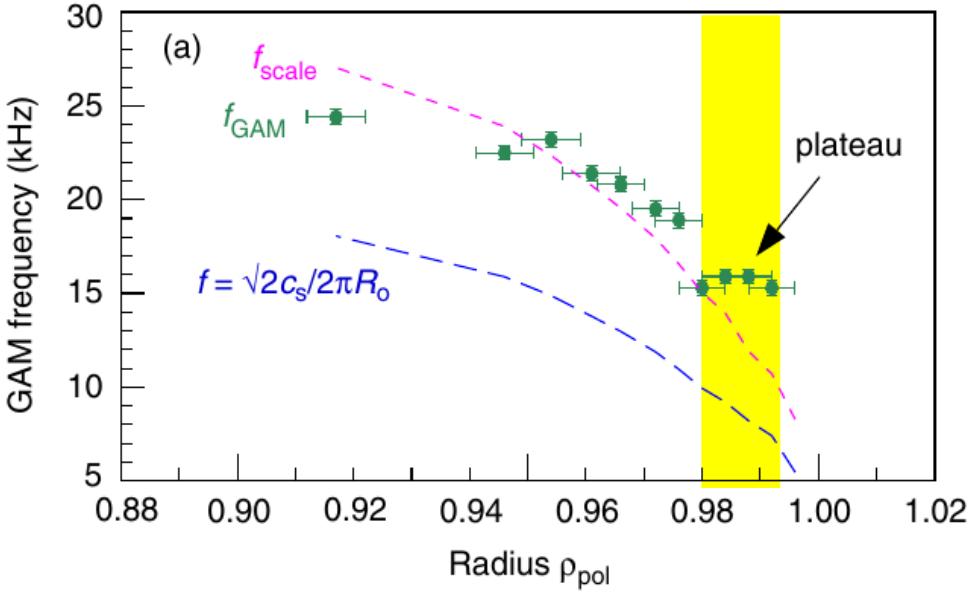


GAM frequency is function of the ion sound velocity

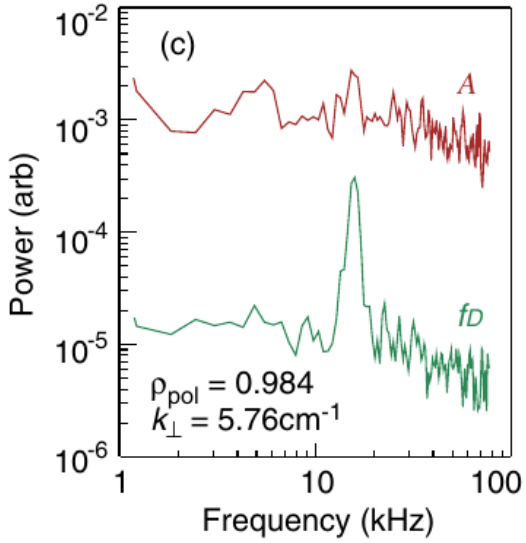


Scattering signal modulus and instantaneous frequency spectrum (Asdex-U)

G. Conway, PPCF (2008)

# Geodesic Acoustic Modes on Tore Supra

GAMs Er x B poloidal velocity oscillation can be directly observed by collective scattering.
Instantaneous Doppler velocity can be extracted from collective scattering signal using MUSIC algorithm (MUltiple SIgnal Classification).

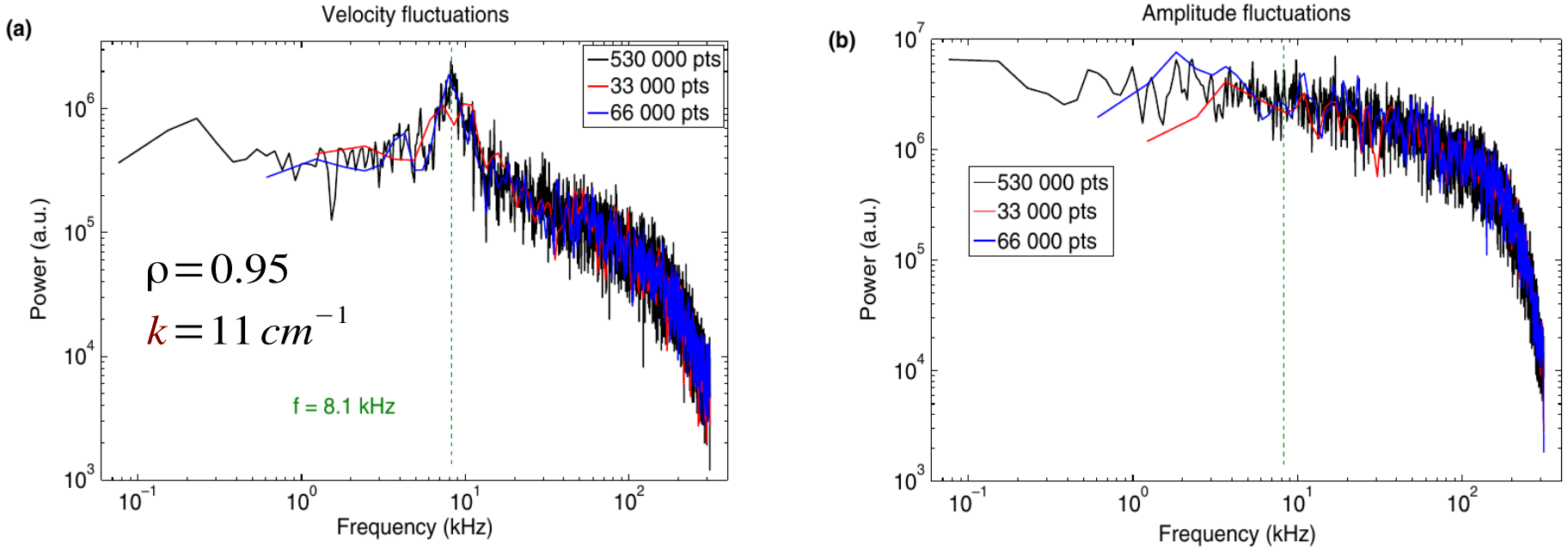


GAM frequency is absent in the scattering signal modulus frequency spectrum.
GAM frequency is observed the instantaneous poloidal velocity frequency spectrum.

L. Vermare et al., PPCF (2012)

# Bibliography

J. Wesson, Tokamaks, 3rd edition, Clarendon Press Oxford (2004)
Chap. 10.10 : Diagnostics - Measurements from fluctuations
I. H. Hutchinson, Principles of Plasma Diagnostics, 2nd ed, Cambridge Univ. Press (2002)
Chap. 7 : Scattering of electromagnetic radiation
D.H. Froula et al., Plasma Scattering of Electromagnetic Radiation, Academic Press, (1975)
Chap. 12 : Scattering from Unstable Plasmas

# Physical constants

$k_B = 1{,}38\ 10^{-23}\ JK^{-1}$ : Boltzmann constant
$h = 6.62\ 10^{-34}\ Js$ : Planck constant
$C = 2{,}99\ 10^{8}\ ms^{-1}$ : speed of light in vacuum
$\varepsilon_0 = 8.85\ 10^{-12}\ Fm^{-1}$ : vacuum permittivity
$\mu_0 = 4\pi\ 10^{-7}\ Hm^{-1}$ : vacuum permeability
$q_e = 1{,}60\ 10^{-19}\ C$ : elementary charge
$m_e = 9{,}11\ 10^{-31}\ kg$ : electron mass
$r_e = \frac{1}{4\pi\epsilon_0}\frac{q_e^2}{m_e C^2} = 2.82\ 10^{-15}\ m$ : electron classical radius
$N_A = 6{,}022\ 10^{23}\ mol^{-1}$ : Avogadro constant
$m_u = 1{,}66\ 10^{-27}\ kg$ : atomic mass unit

- Standard parameters

$T_0 = 273.15\ K$ : standard air temperature ( $0\,^\circ C$ )
$P_0 = 1{,}013\ 10^{5}\ Pa$ : standard air pressure
$n_0 = 2{,}69\ 10^{25}\ m^{-3}$ : ideal gas molecular density at $T_0$ and $P_0$

- Units

$1\ Torr = \frac{1{,}013\ 10^{5}}{760}\ Pa = 133{,}3\ Pa$ : pressure corresponding 1 mm of mercury
$1\ eV = \frac{1{,}6\ 10^{-19}}{1{,}38\ 10^{-23}}\ K = 1{,}16\ 10^{4}\ K$